JB Journals.ASM.org

A Novel C-Terminal Region within the Multicargo Type III Secretion Chaperone CesT Contributes to Effector Secretion

Thangadurai Ramu,[a] Madhulika Esther Prasad,[a] Erica Connors,[a] Amit Mishra,[a] Jenny-Lee Thomassin,[a] Jason Leblanc,[b] Jan K. Rainey,[c,d] Nikhil A. Thomas[a,e]

Department of Microbiology and Immunology, Dalhousie University,[a] Department of Pathology and Laboratory Medicine, Dalhousie University,[b] Department of Biochemistry and Molecular Biology, Dalhousie University,[c] Department of Chemistry, Dalhousie University,[d] and Department of Medicine (Infectious Diseases), Dalhousie University,[e] Halifax, Nova Scotia, Canada

The enteropathogenic *Escherichia coli* (EPEC) multicargo chaperone CesT interacts with at least 10 effector proteins and is central to pathogenesis. CesT has been implicated in coordinating effector hierarchy, although the mechanisms behind this regulation are poorly understood. To address this question, we set out to functionally characterize CesT with respect to roles in (i) effector binding, (ii) effector recruitment to the type III secretion system (T3SS), and (iii) effector translocation into host cells. A CesT variant expression library was screened in EPEC using a newly developed semi-high-throughput secretion assay. Among many deficient CesT variants, a predominant number were localized to a novel CesT C-terminal region. These CesT C-terminal variants exhibited normal effector binding yet reduced effector secretion levels. Structural correlation and thermal spectroscopy analyses of purified CesT variants implicated multiple surface-exposed residues, a terminal helix region, and a flexible C-terminal triple-serine stretch in effector secretion. Site-directed mutagenesis of the flexible CesT C-terminal triple-serine sequence produced differential effector secretion, implicating this region in secretion events. Infection assays further indicated that the C-terminal region of CesT was important for NleA translocation into host cells but was dispensable for Tir translocation. The findings implicate the CesT C terminus in effector secretion and contribute to a model for multiple-cargo chaperone function and effector translocation into host cells during infection.

Many pathogenic bacteria use a type III secretion system (T3SS) to rapidly inject effector proteins into host cells during infection. Effector proteins are synthesized in the bacterial cytosol and are trafficked across the bacterial inner and outer membranes and eventually across the host cell membrane (reviewed in reference 1). Effectors then function to target and subvert host cellular processes often to aid bacterial survival. Effector translocation into host cells is therefore a complex process that requires a macromolecular T3SS structure, which is thought to span three biological membranes when fully assembled.

Additional bacterial proteins are considered ancillary to the T3SS ultrastructure but are critical factors for its biological function to inject effectors into host cells during infection. Type III secretion chaperones (T3SC) do not form part of the T3SS ultrastructure *per se*, although their substrate binding and docking roles at the base of the assembled T3SS are thought to be key events that support effector translocation during infection (2–4). Three classes of T3SC have been identified. There are T3SC that bind effectors (class I), translocon or pore-forming proteins (class II), and needle proteins (class III). Generally, class III needle protein T3SC are thought to prevent premature association or polymerization of monomeric needle proteins within the bacterial cytoplasm (5). Class II T3SC of translocon proteins bind their cargos within the bacterial cell and in many cases are required for translocon protein secretion (6). For effector binding class I T3SC, there are two subclasses: IA and IB (7). Class IA T3SC are thought to bind a single effector, whereas class IB T3SC bind to several effectors. Crystal structures of class IA T3SC from different pathogens display remarkable structural similarity, often forming stable dimers along a helical interface (8, 9). There is a notable absence of significant sequence similarity, although structural folds appear to be well conserved, as T3SC generally exhibit a secondary structure of α-β-β-β-α-β-β-α. As a group of proteins, T3SC are small (15 to 20 kDa) and acidic (pI 4 to 5) and remain within the bacterial cell even after effector cargo has been translocated into a host cell during infection (a possible exception is Spa15 of *Shigella* [10]).

The initial discoveries of T3SC from several laboratories suggested that dedicated or cognate chaperone-effector pairings were common. This was supported by the observation that the genes for the cognate pair were often adjacent to each other and typically shared common transcriptional regulatory control (7, 11, 12). Later on, it became evident that some T3SC bind to multiple effector proteins (reviewed in reference 13). These class IB or multiple-cargo chaperones have been identified and characterized from different bacteria, including pathogenic *Escherichia coli* (CesT), *Shigella* (Spa15), *Salmonella* (InvB and SrcA), *Chlamydia* (McsC), and *Xanthomonas* (HpaB) (4, 14–23). Given that these multiple-cargo chaperones contribute to the biological function of various effectors, it is likely that they play a significant role during infection. This view is supported by the fact that T3SC null mutants are often attenuated in relevant animal or plant models of infection (11, 19, 23, 24).

T3SC have been reported to have a range of functional properties, including roles in transcriptional activation (25, 26), pro-

Received 9 October 2012 **Accepted** 28 November 2012
Published ahead of print 7 December 2012
Address correspondence to Nikhil A. Thomas, n.thomas@dal.ca.
Supplemental material for this article may be found at http://dx.doi.org/10.1128/JB.01967-12.

doi:10.1128/JB.01967-12

tein stability (21, 27, 28), and recruitment or "docking" actions at the base of the T3SS apparatus near the bacterial inner membrane (4, 29). It has also been shown in the case of *Yersinia* that SycE chaperone binding to its partner effector YopE results in a localized conformational change in YopE from a disordered to an ordered state (30). The resulting conformational change is thought to be favorable for presenting YopE to a component of its T3SS (31–33).

The chaperone for *E. coli* secreted protein Tir, CesT, is encoded within an ~35-kb pathogenicity island termed the genetic locus of enterocyte effacement (LEE), which is found in attaching and effacing pathogenic *E. coli* strains (34). CesT was first reported and categorized as a class IA T3SC (21, 22), although later work demonstrated that it also interacts with the enteropathogenic *E. coli* (EPEC) effector Map (14). *In vitro* cell line and animal models of infection have demonstrated that CesT contributes to effector translocation into host cells and is essential for efficient host colonization (21, 24, 35). With the discovery of additional effector proteins encoded outside the LEE pathogenicity island (24, 36), CesT was further shown to bind many non-LEE-encoded (Nle) effectors, and hence it is best categorized as a multicargo T3SC chaperone (4). CesT is known to interact with Tir, Map, EspF, EspH, NleA, EspG, NleG, NleH, NleH2, and EspZ (4, 14, 37). The only other class I T3SC of EPEC is CesF, which binds to EspF (38). It is not known why EspF interacts with both CesT and CesF. The absence of additional EPEC T3SC for its arsenal of effectors (at least 21) (36) is puzzling, since other pathogens often display distinct chaperone-effector pairings (e.g., *Yersinia* [YopE/SycE, YopT/SycT, YopO/SycO, and YopH/SycH], *Salmonella* [SptP/SicP and SigD/SigE], and *Shigella* [IcsB/IpgA and IpgD/IpgE]). There is the possibility that CesT represents a "general-purpose" multiple-cargo T3SC or, alternatively, that additional EPEC T3SC exist but remain to be discovered.

CesT (156 amino acids [aa]) forms stable 34.5-kDa homodimers in solution as determined by equilibrium sedimentation analysis (8). Furthermore, static light scattering experiments with a Tir/CesT complex indicated that CesT binds to Tir in a probable 2:1 ratio. A degenerate chaperone binding domain (CBD) has been identified within some EPEC effectors, which partially addressed how CesT physically interacts with different effector proteins (39). Mutational analyses have implicated certain CesT amino acid residues and a coiled-coil domain in substrate binding to its prototypic effector partner Tir (8, 40). CesT has been implicated in mediating hierarchical effector secretion, although the underlying mechanism remains unknown (39). Here, using a CesT variant expression library and a newly designed functional secretion assay, we have identified a novel C-terminal region of CesT (absent from other T3SC) as an important factor in EPEC effector secretion.

MATERIALS AND METHODS

Growth of bacterial strains. The bacterial strains used and generated in this study are listed in Table 1. Bacteria were routinely cultured in Luria broth (LB) (1% [wt/vol] tryptone, 0.5% [wt/vol] yeast extract, 1% [wt/vol] NaCl) at 37°C. Antibiotics (Sigma) were added when appropriate to a final concentrations of 50 μg/ml kanamycin, 50 μg/ml streptomycin, 30 μg/ml chloramphenicol, 200 μg/ml ampicillin, and 10 μg/ml tetracycline.

Recombinant DNA techniques. The pCesT plasmid was generated by cloning a DNA fragment carrying the *cesT* allele into the mobilizable broad-host-range plasmid pRK415 (41). Briefly, primers CesTFOR2 and CesTREV (Table 2) were used in a PCR with EPEC genomic DNA as the template. The resulting fragment was cloned into Eco53kI-treated pRK415 to generate pCesT. A sequence of a suitable ribosome binding site was also included (within primer CesTFOR) to ensure CesT expression. This recombinant construct expresses untagged CesT, transcribed from the *lac* promoter within the pRK415 vector. Our efforts to generate a plasmid that encodes CesT from the native *cesT* LEE5 EPEC promoter were not successful for unknown reasons (data not shown).

A *cesT1* strain expressing CesT(S147A) from the *cesT* chromosomal locus was generated by replacing the *cesT* allele using allelic exchange as previously described (42). Briefly, two separate PCRs with primer pairs NT265-NT247 and NT266-NT246 were performed, each using pCesT as the template DNA. Phusion DNA polymerase was used to generate blunt-ended DNA amplification products that were subsequently purified, treated with T4 polynucleotide kinase, and blunt-end ligated with T4 DNA ligase to generate DNA hybrids. The ligated DNA served as the template in a PCR with primers NT265 and NT266. The resulting amplicon that formed *cesT*(S147A) was digested with SacI and KpnI, followed by cloning into SacI- and KpnI-treated pRE112. The resulting pRE112-based suicide construct (pΔS147A) was mated into wild-type and Δ*sepD* mutant EPEC and subjected to allelic exchange followed by sucrose selection. Individual *cesT1* or Δ*sepD cesT1* clones were identified by PCR and DNA sequencing analyses. A similar approach with cloning and allelic exchange was used to generate the Δ*sepD cesT2* mutant, which expresses CesT(H128R) from the *cesT* chromosomal locus. All newly generated DNA constructs in this study were sequenced at the McGill University and Genome Quebec Innovation Centre.

EP-PCR and site-directed mutagenesis of the *cesT* allele. A cloned wild-type EPEC *cesT* allele (468 bp) within pCesT was used as the DNA template in error prone PCR (EP-PCR) to generate a variant *cesT* allele library. EP-PCR was carried out with *Taq* DNA polymerase (NEB Canada, catalogue number M0273L) and $MnCl_2$ under conditions empirically demonstrated to generate 1 mutation in approximately 450 bp of extension products (43), with some modifications. An EP-PCR buffer (10×; 70 mM $MgCl_2$, 500 mM KCl, 100 mM Tris-HCl, 0.01% [wt/vol] gelatin, pH 8.3) was used with the following recipe for a 100-μl mixture: 10 μl of 10× EP-PCR buffer, 100 pmol of primer cesTmut-FOR, 100 pmol of primer cesTmut-REV, 100 ng pCesT, 2 μl of 10 mM deoxynucleoside triphosphate (dNTP), 1.6 μl of 10 mM dCTP, 1.6 μl of 10 mM dTTP, 1 μl of *Taq* DNA polymerase, 1.5 μl of 10 mM $MnCl_2$, and 79.3 μl of distilled water (dH_2O). The reaction mixture was divided into 10 tubes (10 μl each) to prevent overrepresentation of single mutations in the library. The tubes were subjected to the following thermocycling conditions on an Eppendorf Mastercycler: 95°C for 3 min; 20 cycles of 94°C for 30 s, 50°C for 45 s, and 72°C for 1 min); and 72°C for 5 min. At the end of the thermocycling, the individual reaction mixtures were pooled and frozen at −20°C. This was repeated 9 mores times to generate a large library of mutated *cesT* DNA fragments. The entire collection of mutated *cesT* DNA fragments (approximately 1 ml) was combined and then purified using a Qiagen PCR purification kit. The purified DNA fragments were treated with SacI and EcoRI and ligated to into pRK415 treated with the same enzymes. The entire ligation mixture (in aliquots) was heat shocked into chemically competent DH5α, followed by selection of transformants on tetracycline medium. Approximately 10,000 transformants were isolated to establish a CesT variant expression library. Using this cloning strategy, directionally cloned *cesT* alleles would be transcribed from the *lac* promoter within pRK415. These transformants were then used in triparental matings to mobilize the recombinant plasmids into the Δ*sepD* Δ*cesT* mutant for phenotypic analyses (see section below).

To generate site-specific mutations, a ligation PCR strategy using oligonucleotides with the desired mutations (Table 2) was used. The mutations were introduced either using engineered in-frame restriction enzyme recognition sequences or by blunt end ligations. Briefly, for each site-specific mutation, Phusion DNA polymerase (Finnzymes) was used with pCesT as the DNA template to generate two PCR products. The PCR products were mixed together, purified, and then treated with the corresponding restriction enzyme or T4 polynucleotide kinase (if blunt-end ligation was required). The digestions or kinase reaction mixture was heat

TABLE 1 Strains and plasmids used in this study

Strain or plasmid	Description	Reference or source
Strains		
Wild-type EPEC strain E2348/69	Streptomycin resistant	39
Δ*sepD* mutant	*sepD* deletion mutant	41
Δ*cesT* mutant	*cesT* deletion mutant	4
Δ*sepD* Δ*cesT* mutant	Double mutant derived from Δ*sepD* mutant	4
Δ*sepD* Δ*cesT*::*cesT*(S147A) mutant	*cis*-complemented strain expressing CesT(S147A)	This study
Δ*cesT*::*cesT*(S147A) mutant	*cis*-complemented strain expressing CesT(S147A)	This study
Δ*escN* mutant	*escN* deletion mutant	42
SM10λ*pir*	*E. coli* strain permissive for pRE112 replication	
DH5α	*E. coli* strain used for cloning	
DH5αλpir	*E. coli* strain used for cloning, permissive for pRE112 replication	
MT616	*E. coli* conjugation helper strain	
BL21(λDE3)	*E. coli* strain used for pET vector-based protein overexpression	Novagen
Plasmids		
pET21a+	T7/His-tagged fusion vector	Novagen
pRK415	Broad-host-range conjugative plasmid	
pΔS147A	Suicide construct to generate *cesT*::*cesT*(S147A)	This study
pCesT	*cesT* allele cloned into pRK415, transcribed from the *lac* promoter	This study
pCesT(E35V/E107G)	Encodes CesT variant, cloned into pRK415	This study
pCesT(P63T)	Encodes CesT variant, cloned into pRK415	This study
pCesT(E68V)	Encodes CesT variant, cloned into pRK415	This study
pCesT(N73T)	Encodes CesT variant, cloned into pRK415	This study
pCesT(L97-stop)	Encodes CesT truncated variant	This study
pCesT(K108E, S147A)	Encodes CesT variant, cloned into pRK415	This study
pCesT(S119P)	Encodes CesT variant, cloned into pRK415	This study
pCesT(H128R)	Encodes CesT variant, cloned into pRK415	This study
pCesT(H128Y)	Encodes CesT variant, cloned into pRK415	This study
pCesT(N129S)	Encodes CesT variant, cloned into pRK415	This study
pCesT(S147G)	Encodes CesT variant, cloned into pRK415	This study
pCesT(S145A)	Encodes CesT variant, cloned into pRK415	This study
pCesT(S145T)	Encodes CesT variant, cloned into pRK415	This study
pCesT(S145E)	Encodes CesT variant, cloned into pRK415	This study
pCesT(S146A)	Encodes CesT variant, cloned into pRK415	This study
pCesT(S146T)	Encodes CesT variant, cloned into pRK415	This study
pCesT(S146E)	Encodes CesT variant, cloned into pRK415	This study
pCesT(S147A)	Encodes CesT variant, cloned into pRK415	This study
pCesT(S147T)	Encodes CesT variant, cloned into pRK415	This study
pCesT(S147E)	Encodes CesT variant, cloned into pRK415	This study
pCesT(1-145aa)	Encodes CesT variant, cloned into pRK415	This study
pHis-CesT	*cesT* cloned in pET28, expresses His-CesT	This study
pHis-CesT(E35V/E107G)	Encodes His-CesT variant	This study
pHis-CesT(P63T)	Encodes His-CesT variant	This study
pHis-CesT(E68V)	Encodes His-CesT variant	This study
pHis-CesT(N73T)	Encodes His-CesT variant	This study
pHis-CesT(L97-stop)	Encodes His-CesT variant	This study
pHis-CesT(K108E,S147A)	Encodes His-CesT variant	This study
pHis-CesT(S119)	Encodes His-CesT variant	This study
pHis-CesT(H128R)	Encodes His-CesT variant	This study
pHis-CesT(H128Y)	Encodes His-CesT variant	This study
pHis-CesT(N129S)	Encodes His-CesT variant	This study
pHis-CesT(S147G)	Encodes His-CesT variant	This study
pHis-CesT(1-145aa)	Encodes His-CesT variant	This study
pNleA-FLAG	pACYC184 with cloned *nleA* allele, expresses NleA-FLAG from the *nleA* promoter	39

inactivated and then treated with T4 DNA ligase for 1 h at room temperature. The resulting ligation reaction mixture was diluted 10-fold and then used as the template in a PCR with primers cesTmutF and cesTmutR. The resulting PCR products were digested with SacI and EcoRI and then directionally cloned into pRK415. Following transformation into DH5α, recombinant plasmids were screened for the engineered restriction site as determined by restriction enzyme digestion. All site-directed mutagenesis plasmid constructs were verified by sequencing and then mobilized into appropriate EPEC strains by conjugation.

Semi-high-throughput conjugation to generate a CesT variant expression library. A triparental mating was performed to mobilize the *cesT* allele library into the EPEC Δ*sepD* Δ*cesT* double mutant. Briefly, variant

TABLE 2 Oligonucleotide primers used in this study

Primer	Sequence	Use
NT242	CCG CTA GCA GCG ATA ATA AAC ATT ATT ACG C	CesT(S145A)
NT243	CCG CTA GCA ATT TCC TCT ATT TTC ATA TGT TCG	CesT(S145A)
NT244	CCG CTA GCG ATA ATA AAC ATT ATT ACG CC	CesT(S146A)
NT245	CCG CTA GCG CTA ATT TCC TCT ATT TTC ATA	CesT(S146A)
NT246	GCC GAT AAT AAA CAT TAT TAC GCC GG	CesT(S147A)
NT247	TGA GCT AAT TTC CTC TAT TTT CAT ATG	CesT(S147A)
NT248	GGA CTA GTA GCG ATA ATA AAC ATT ATT ACG	CesT(S145T)
NT249	GGA CTA GTA ATT TCC TCT ATT TTC ATA TGT TCG	CesT(S145T)
NT250	GGA CTA GTG ATA ATA AAC ATT ATT ACG CC	CesT(S146T)
NT251	GGA CTA GTG CTA ATT TCC TCT ATT TTC ATA	CesT(S146T)
NT252	ACC GGT CGA CCG ATA ATA AAC ATT ATT ACG CC	CesT(S147T)
NT254	CCG ATA TCA AGC GAT AAT AAA CAT TAT TAC G	CesT(S145E)
NT255	TCA ATT TCC TCT ATT TTC ATA TGT TCG	CesT(S145E)
NT256	CCG ATA TCC GAT AAT AAA CAT TAT TAC GCC	CesT(S146E)
NT257	TCG CTA ATT TCC TCT ATT TTC ATA TG	CesT(S146E)
NT258	GAT AAT AAA CAT TAT TAC GCC G	CesT(S147E)
NT259	CCG AGC TCT GAG CTA ATT TCC TCT ATT TTC ATA TG	CesT(S147E)
NT260	TGT GAG TTA GCT CAC TCA TTA GG	pRK415
NT261	TCG ACG CTC AAG TCA GAG GTG GCG	pRK415
NT262	ACC GGT CGA CGA AAT TTC CTC TAT TTT CAT ATG	CesT(S147T)
NT265	CCG AGC TCA CTG GTC AGA TTC CTC TAG CG	*cesT1* with NT247
NT266	CCG GTA CCG CCT GCA ACT GTG ACG AAG CC	*cesT1* with NT246
NT295	TAC GTA ATA CCA AAT ACA GAT T	*cesT2* with NT247
NT296	GGG AAT AAC ATT AGA AAA CG	*cesT2* with NT246
cesTmutF	CCG AGC TCT TAA GAA GGA GAT ATA CCA TG	Error-prone PCR
cesTmutR	AAG AAT TCG TAA ATT AAT ACT AAT AAA TAA GTT TTA	Error-prone PCR
CesT-FOR2	CCG AGC TCT TAA GAA GGA GAT ATA CCA TGT CAT CAA GAT CTG AAC TTT TAT TAG	pCesT
CesT-REV	CCG AGC TCG TAA ATT AAT ACT AAT AAA TAA GTT TTA	pCesT

cesT alleles cloned into pRK415 and hosted within DH5α (donors) were grown overnight in LB within 96-well plates. The next day, 100 μl of molten LB agar was added to each well of a new 96-well plate to create a solid nutrient surface favorable for conjugation. Portions of 25 ml of overnight cultures of *E. coli* MT616 (conjugative helper) and EPEC Δ*sepD* Δ*cesT* (recipient) were mixed together and pelleted by centrifugation, followed by resuspension in 12.5 ml of fresh LB. Fifty microliters of the helper-recipient mixture was added to each well of the 96-well LB agar plate. Twenty-five microliters of each donor strain was added to individual wells using a multichannel pipettor. The 96-well plate was incubated at 37°C for 1.5 h. Two hundred microliters of fresh LB was added to each well to resuspend the bacteria. A pipette tip-loaded multichannel pipettor was then dipped into the wells of the plate and then used to inoculate a fresh 96-well plate containing liquid LB with streptomycin and tetracycline to select for recipient strains that had received the donor plasmid encoding tetracycline resistance. This growth medium also selected against donor and helper strains as determined by control experiments. After overnight growth, the individual cultures were streak purified onto LB agar petri plates with streptomycin and tetracycline. Streak-purified single colonies were inoculated in multiwell plates with LB plus antibiotics, followed by another incubation at 37°C to establish the CesT variant expression library. Glycerol (15%, vol/vol) was added to the multiwell plates, followed by freezing at −80°C until expression studies.

***In vitro* and semi-high-throughput secretion assays.** A standard *in vitro* secretion assay protocol (in 6-well microplates) was performed as previously described (4). For secreted protein and whole-cell lysate analyses by SDS-PAGE and immunoblotting, the standard protocol was used. For semi-high-throughput assays, the standard protocol was modified so that quantitative absorbance values could be obtained using a modified Bradford protocol (44). Briefly, overnight cultures of EPEC strains were subcultured (1/50) into 24-well plates. Each well contained 1 ml of prewarmed Dulbecco modified Eagle medium (DMEM) (Invitrogen). The plate was incubated for 6 to 6.5 h at 37°C and 5% CO_2 with static growth. Eight hundred microliters of each culture was pelleted (5 min at 13,200 rpm; Eppendorf 5424) in microcentrifuge tubes. Exactly 500 μl of the resulting supernatants was quickly transferred to cuvettes containing 500 μl Coomassie blue protein assay reagent (Thermo Scientific, product number 1856209). The supernatant-Coomassie blue reagent mixtures were gently mixed and incubated at room temperature for 20 min. The cuvettes were then placed in an Eppendorf Biophotometer set to read absorbance at 595 nm. A 1:1 mixture of DMEM-Coomassie blue reagent served to blank the instrument. The Δ*sepD*, Δ*sepD* Δ*cesT*, and Δ*sepD* Δ*cesT*/pCesT strains were included in each plate assay as controls. Readings were taken twice to assess reproducibility of the absorbance values (see Fig. S1 in the supplemental material for a flowchart of the assay). A standard curve for bovine serum albumin-diluted DMEM was generated to determine the linear range of the modified Bradford assay. The assay as performed (500 μl of secreted fraction sample mixed with 500 μl of reagent) fell within the linear range of detection. Typical values for absorbance of EPEC Δ*sepD* were 0.35 to 0.4, corresponding to 15 to 20 μg/ml of protein. EPEC strains with deficiencies in CesT function typically produced a secreted fraction absorbance of 0.2 to 0.3, or 5 to 10 μg/ml protein.

Bioinformatic analysis and structure-function correlation of CesT variants. Selected CesT variants (from a subset of 142 isolates) were followed up with detailed analyses. The rationale for selection was based on grouping the 142 encoded CesT variants into three separate and identifiable groups: (i) CesT dimerization interface, (ii) surface exposed on the CesT homodimer, and (iii) potential CesT intramolecular interaction. Cases where multiple mutations in the *cesT* allele were observed were not followed up (a few isolates were followed to learn more about isolates with single mutations that were in common). Representative sets of isolates were selected for detailed biochemical analyses and form the data within this report.

All structure-function analyses was carried out on the nuclear magnetic resonance (NMR) spectroscopy-derived CesT homodimer structural model (the Protein Data Bank [PDB] coordinate file was kindly provided by Markus Zweckstetter, Max Planck Institute for Biophysical Chemistry, Göttingen, Germany) (45), based upon the domain-swapped X-ray structure of *E. coli* CesT (PDB entry 1K3E). Structural analysis was not carried out on sections of the CesT homodimer involved in the domain swap in the original crystal structure. Instead, inferences about surface accessibility and residue positioning were made, where possible, by considering the proximal unswapped portion of CesT. Molecular visualization and image production were performed using MacPyMol (Schrödinger LLC, Portland, OR).

Protein sequences were subjected to COBALT (constraint-based alignment tool) (46), which uses conserved domain database (CDD) information along with PROSITE protein motif database information to produce multiple-sequence alignments.

EPEC type III effector translocation assays. A quantitative assay for Tir-mediated actin reorganization (binding index) was performed on HeLa or HT29 cells using the method described by Vingadassalom et al. (47), with detection by fluorescent phalloidin staining as previously described (42). To detect Tir and NleA protein translocation resulting from EPEC infection, HeLa cells were mechanically fractionated and immunoblotted with appropriate antibodies, as previously demonstrated (48). All translocation experiments were performed at least three times, with representative data shown.

CesT-type III effector protein binding assay. A CesT affinity column binding assay was performed as previously described (39). Freshly purified His-CesT was exposed to 1 ml of filtered (0.22-μm pore size, low protein binding; Millipore) Δ*sepD* culture supernatant, which contains an abundance of secreted EPEC type III effectors (49). After 1 h of rotation on a Labquake rotator at room temperature, the microcentrifuge tubes were centrifuged (3,000 rpm; Eppendorf 5415D) to pellet the resin. Unbound proteins (supernatant) were removed, followed by three washes with wash buffer to reduce nonspecific protein or resin interactions. Empty resin (no His-CesT) served as a control. Bound proteins were coeluted from the resin (with His-CesT). The eluted fractions were precipitated using trichloroacetic acid and processed for SDS-PAGE.

Protein overexpression and purification. Recombinant plasmids with various cloned *cesT* alleles were introduced into *E. coli* BL21(λDE3). Bacterial strains were cultured in LB at 37°C (200 rpm) until reaching an optical density at 600 nm (OD_{600}) of 0.6 and then induced for protein expression by adding 0.1 mM isopropyl-β-D-thiogalactopyranoside (IPTG). Cultures were further incubated for 2.5 h, followed by harvesting the bacterial cells by centrifugation. The resulting bacterial pellets were either used immediately or stored at −20°C.

Soluble histidine-tagged CesT and CesT variants were purified using Ni-nitrilotriacetic acid (NTA) resin (Qiagen) as previously described (4).

Differential scanning fluorimetry (DSF) analyses. Purified His-CesT or His-CesT variants were used at a final concentration of 1 μM in 20 mM phosphate buffer (pH 7.5), 150 mM NaCl, and 10 mM EDTA. One microliter of a 25× Sypro orange solution (Invitrogen) was added to the respective sample reactions. Reaction mixtures were added in 25-μl volumes to glass capillaries and placed onto a LightCycler 2.0 instrument (Roche Diagnostics). Melting curve analysis was performed by increasing the temperature from 37°C to 95°C with a ramp rate of 0.05°C/s. During thermal denaturation, continuous fluorescence was captured in all channels. Data were analyzed by using melting temperature (T_m) analysis software provided by the manufacturer (version 4.05). The raw data captured from the 610-nm channel were exported and reanalyzed using the Multicode-RTx analysis software version 1.6.4.1 (Eragen BioSciences). Threshold values for baseline fluorescence were set to values obtained for the negative controls (Sypro orange alone and proteins alone). Crystalline hen egg lysozyme (Sigma) dissolved in the same reaction buffer was used as a control.

Protein and immunoblotting techniques. SDS-PAGE was carried out by the method of Laemmli (50) with minor modifications using a Bio-Rad mini-Protean system under constant voltage. Protein transfer to membrane supports (polyvinylidene difluoride [PVDF]; Millipore) was performed using a semidry transfer apparatus operating at 15 V, and immunoblotting was carried out as previously described (42). Antibodies were used at the following dilutions; anti-EscJ, 1:500 (51); anti-FLAG, 1:10,000 (Sigma); anti-RNA polymerase, 1:2,000 (Santa Cruz Biotechnology); anti-calreticulin, 1:5,000 (Calbiochem); antitubulin, 1:5,000 (Calbiochem); anti-Tir, 1:1,000 (39); goat anti-mouse conjugated to horseradish peroxidase (HRP), 1:5,000 (Rockland Immunochemicals); goat anti-rabbit conjugated to HRP, 1:5,000 (Rockland Immunochemicals); and goat anti-rat conjugated to HRP, 1:5,000. Monospecific affinity-purified anti-CesT antibodies raised against a synthetic peptide (LENEHMKIEEISSS DNK) that corresponds to the C-terminal region of CesT (42) were used at a 1:10,000 dilution. For immunoblot detection, an Immun-Star WesternC kit (Bio-Rad) was used as directed by the manufacturer. Chemiluminescent signals were captured using a Bio-Rad VersaDoc MP5000 as previously described (42) and normalized to control protein signals within the same sample. All measurements were made within the linear range of detection for each antibody and processed for densitometry using Image Lab software (version 4.1).

RESULTS

Development of a new semi-high-throughput secretion assay to evaluate CesT function. Bioinformatics approaches have been effective at identifying effectors and T3SC within bacterial genomes (52–54) although there are currently no functional screens that effectively assess T3SC function *in vivo*. We therefore set out to design a genetic and biochemical screen to assess CesT function in EPEC. The secretion profiles of *cesT* mutants contain considerably reduced amounts of effector proteins (4). Furthermore, in a Δ*sepD* genetic background, which is known to support high levels of effector secretion, the additional deletion of *cesT* (i.e., Δ*sepD* Δ*cesT*) results in bacteria that are deficient in effector secretion (4). The *sepD* mutant also has low-level translocator secretion, which is critical to this assay since normal levels of translocator secretion would obscure any decreased effector levels. Therefore, we took advantage of the reduced effector protein amounts within culture supernatants of a Δ*sepD* Δ*cesT* double mutant and used this strain to express a CesT variant library generated by error-prone PCR. Typically, to evaluate EPEC *in vitro* type III secretion, we and other groups have precipitated culture supernatants and assessed protein profiles by SDS-PAGE. Such an approach was not feasible for a library screen. We therefore developed a protocol to quantitatively measure total protein amounts in culture supernatants using a common Coomassie blue dye binding assay (see Materials and Methods). Culture supernatants of Δ*sepD*, Δ*sepD* Δ*cesT*, and Δ*sepD* Δ*cesT*/pCesT strains were collected, clarified by centrifugation, and then added to Coomassie blue dye. The amount of protein in the sample was determined by measuring the OD_{595}. As shown in Fig. 1A, the Δ*sepD* Δ*cesT* double mutant exhibited a significant reduction in protein amount in culture supernatants compared to the Δ*sepD* strain (~65% reduction). Genetic complementation of Δ*sepD* Δ*cesT* with a plasmid expressing CesT restored the total secreted protein amount to 85% compared to that for Δ*sepD*, indicating that under these conditions, CesT contributed to the protein amounts observed in culture supernatants and confirming previous findings (4). With this biochemical assay optimized, we proceeded to use conjugation to mobilize and establish a CesT variant plasmid library in the Δ*sepD* Δ*cesT* strain. Using a semi-high-throughput secretion assay protocol, we eval-

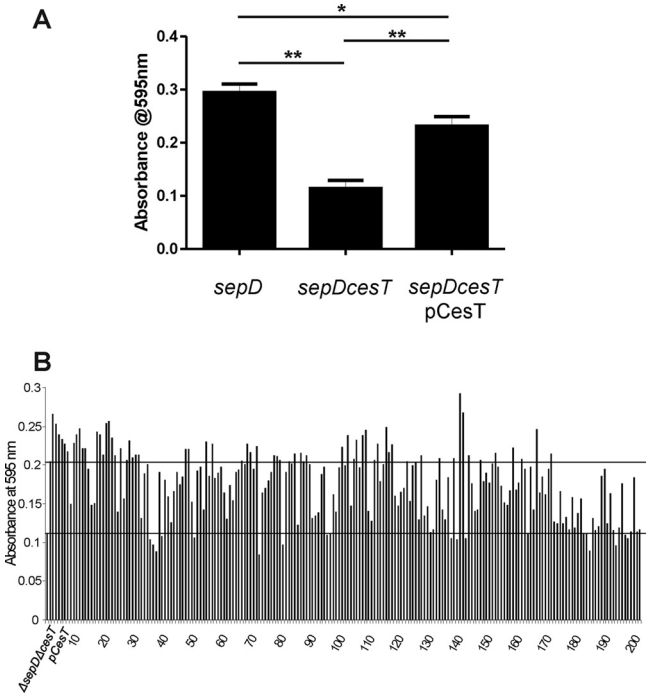

FIG 1 Quantification of total secreted proteins found in culture supernatants using a simple Bradford assay. (A) The high level of total secreted proteins in a Δ*sepD* strain is dependent on CesT. *trans*-complementation of the Δ*sepD* Δ*cesT* double mutant with a plasmid expressing CesT restores high-level secretion to ~85% relative to that for the Δ*sepD* strain. A paired *t* test was used to compare the data, with a two-tailed *P* value being reported. **, $P < 0.0001$; *, $P = 0.0001$. (B) Screening of 200 Δ*sepD* Δ*cesT* library clones that express CesT variants generated by error-prone PCR. Each bar represents the average for an individual clone in two separate experiments. The top and bottom horizontal lines represent the absorbance (protein amount) for the plasmid-*trans*-complemented and noncomplemented Δ*sepD* Δ*cesT* double mutant, respectively. Values below the top line are considered to indicate deficiency for normal CesT function.

uated 1,092 different isolates and quantitatively determined protein amounts in culture supernatants. Approximately 68% of the CesT variants showed a deficiency in restoring protein amounts in culture supernatants back to Δ*sepD* Δ*cesT*/pCesT levels (Fig. 1B, which shows data for 200 isolates). These data suggest that this new semi-high-throughput approach was useful in identifying CesT variants deficient for CesT function.

Isolation and characterization of CesT variants deficient in supporting type III secretion. The strains that displayed reduced protein amounts in culture supernatants were isolated from the library and further characterized ($n = 739$) (see Fig. S2 in the supplemental material for a graphical summary of the data). There still remained the possibility that a Δ*sepD* Δ*cesT* strain could harbor a plasmid with a missense mutation in *cesT* (brought about by error-prone PCR) or that the CesT variant was unstable, not expressed at all, or expressed at levels below those for normal CesT. To identify clones that expressed a CesT variant and displayed reduced amounts of secreted proteins in culture supernatants, whole-cell lysates of the isolated clones were assayed for CesT protein levels using immunoblotting with anti-CesT antibody. Using this approach, we determined that 92% ($n = 680$) of the clones with reduced protein amounts in culture supernatants did express a CesT variant (Fig. 2A shows an example). A few clones displayed slower CesT migration in SDS-PAGE, a feature that has been observed before for other CesT variants (8). Rarer cases of CesT variants with faster migration in SDS-PAGE were also observed (Fig. 2A). To assess effector steady-state intracellular levels, whole-cell lysates (harvested after 6 h postinoculation in DMEM) were probed with anti-Tir and anti-NleA antibodies. These two effectors are known to interact with CesT (4). Some Δ*sepD* Δ*cesT* strains expressing CesT variants had marked reductions in Tir intracellular steady-state levels compared to that supported by wild-type CesT (Fig. 2B). Immunoblotting with anti-NleA polyclonal sera was challenging due to background signals, although it was possible to determine that NleA intracellular levels were reduced for all Δ*sepD* Δ*cesT* strains expressing CesT variants compared to normal CesT. We considered these altered Tir and NleA steady-state intracellular levels as phenotypic evidence for altered CesT function (discussed in context of CesT substitution below).

Under secretion-inducing conditions, the most abundant proteins within EPEC Δ*sepD* culture supernatants are effector proteins (49). Importantly, mass spectrometry analyses have characterized and identified the protein species (4, 39). Therefore, Δ*sepD* secreted protein profiles (and genetic derivatives) can be compared with respect to protein species content and abundance. From the 680 isolates, 100 random isolates were selected, and their secreted proteins were compared to those of the Δ*sepD* Δ*cesT*/pCesT strain by Coomassie blue staining and immunoblotting. Some isolates were found to not support efficient effector secretion and appeared to be similar to the Δ*sepD* Δ*cesT* strain, whereas others demonstrated an overall reduced level of effector secretion compared to that for the Δ*sepD* Δ*cesT*/pCesT strain (Fig. 2D shows data for 12 selected isolates). The majority of isolates demonstrated a pattern of differential effector secretion, that is, where the levels of Tir effector were reduced and NleA effector was absent as detected by immunoblotting of secreted protein fractions (Fig. 2E and F).

Allelic replacement of chromosomal *cesT* with modified *cesT* alleles validates the library screen. *trans*-complementation of the Δ*sepD* Δ*cesT* mutant strain with a plasmid expressing CesT restored secretion efficiency to ~85% of that for the Δ*sepD* strain (Fig. 1A), and the phenotypic characterization of strains expressing *trans*-complemented CesT variants showed altered secretory profiles (Fig. 2D). To validate our genetic screen and to rule out overexpression and plasmid expression artifacts, we generated *cis*-complemented strains by replacing chromosomal *cesT* with altered *cesT* alleles. Instead of CesT(S147G), we generated the Δ*sepD cesT1* strain, expressing CesT(S147A) (discussed for other experiments described below), and the Δ*sepD cesT2* strain, expressing CesT(H128R). As expected, these strains exhibited similar altered secretory phenotypes (Fig. 3A and B) compared to the Δ*sepD* Δ*cesT trans*-complemented strains. These data suggest that the library screen was efficient in identifying CesT variants deficient in effector secretion. Therefore, the plasmids from 100 Δ*sepD* Δ*cesT* mutant strain isolates were collected and subjected to DNA sequencing to determine the corresponding mutation.

Structural correlation analyses locate surface-exposed amino acid residues and a C-terminal region that contribute to CesT function. From the isolated CesT variants deficient in normal effector secretion, we formed three defined groups, based on where the mapped mutation was found on the CesT homodimer: (i) dimerization interface, (ii) surface exposed, and (iii) intramolec-

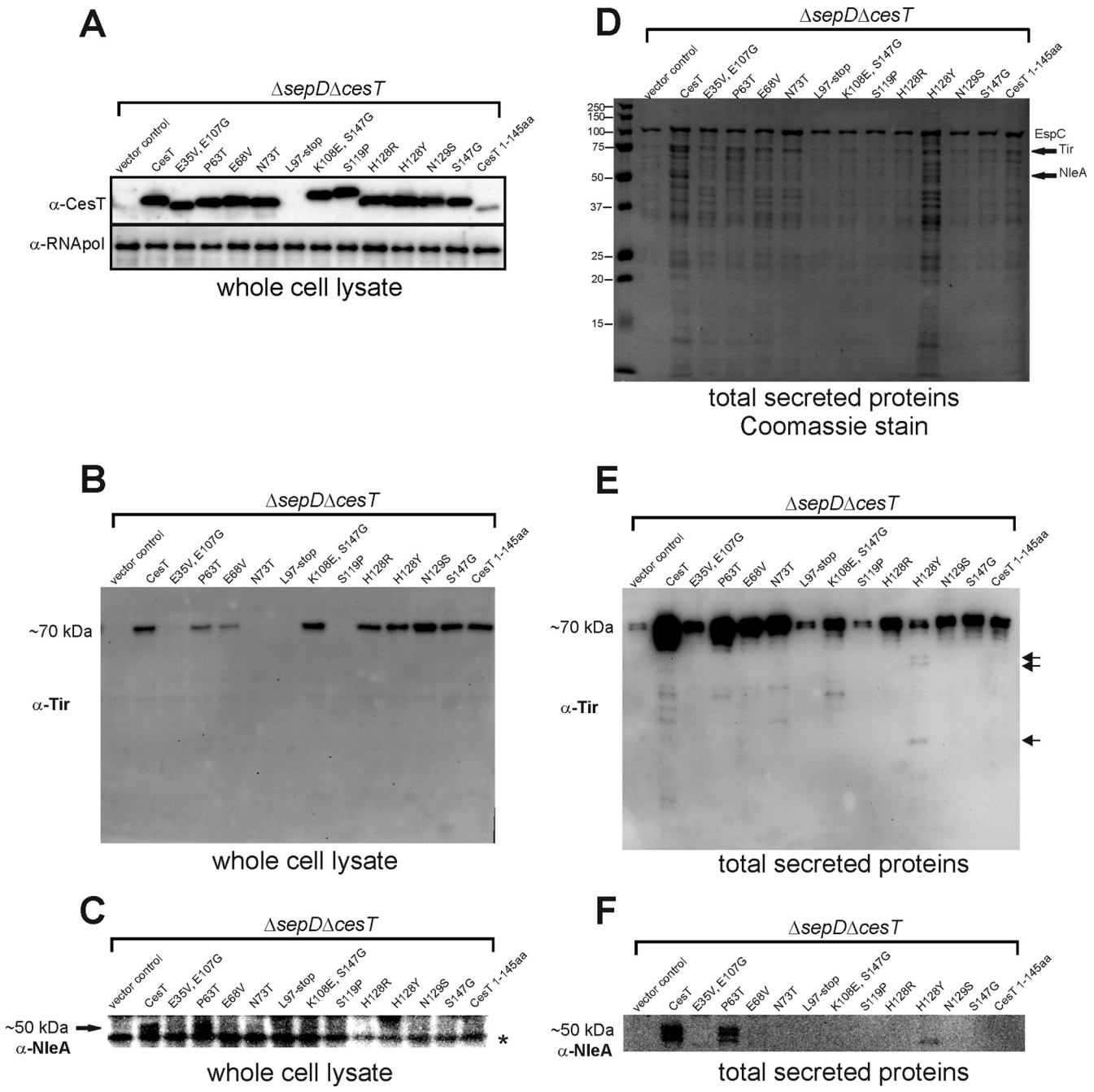

FIG 2 Characterization of selected CesT variants isolated from a genetic screen for type III effector secretion levels. (A) Immunoblot of whole-cell lysates. Anti-RNA polymerase antibodies served as a loading control to demonstrate relative loading of whole-cell lysates. Monospecific anti-CesT antibodies raised against a short C-terminal CesT peptide (aa 135 to 156) detect the C-terminal region of CesT. A weaker signal is observed for CesT(Δ145-156), presumably due to a lower level of antibody binding. (B and C) Immunoblots to detect Tir and NleA effector intracellular steady-state protein levels for specific CesT variants. The arrow in panel C points to NleA, and the asterisk indicates a nonspecific cross-reactive protein species found in all samples. (D) Total secreted protein profiles from Δ*sepD* Δ*cesT* strains harboring different CesT variants were stained with Coomassie blue G-250. The locations of Tir and NleA protein species are known from previous mass spectrometry studies. Some protein species within the secreted protein preparations are partially degraded effector proteins. The arrows point to the known positions of "intact" Tir and NleA effectors in the respective samples. EspC is a type V secreted protein and is not CesT dependent (remains unchanged in a Δ*sepD* Δ*cesT* double mutant), and it therefore served as a loading control for each total secreted protein preparation. (E and F) Anti-Tir and anti-NleA immunoblots of total secreted proteins collected from Δ*sepD* Δ*cesT* strains expressing CesT variants. The arrows in panel E indicate novel Tir degraded products for CesT(H128Y).

ular interaction. We expand on selected amino acids substitutions in the context of the known CesT crystal and NMR structures in the following section.

Three amino acid substitutions, P63T, E68V, and N73T, are near or within the helical CesT dimerization interface α2. Proline 63 and asparagine 73 are paired symmetrically with the corresponding residue in the other monomer, such that a replacement by threonine would increase bulk and potentially disrupt efficient

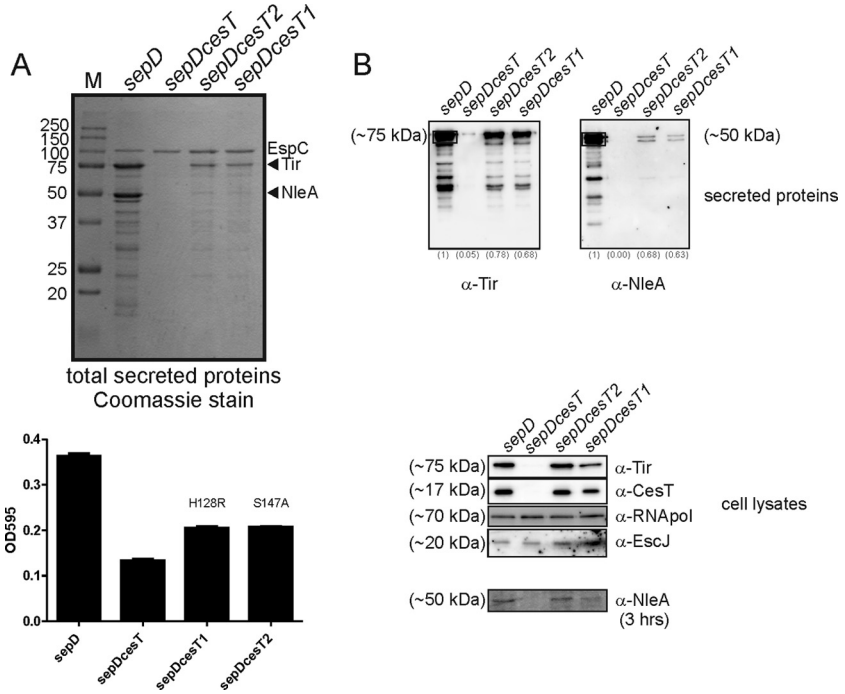

FIG 3 Δ*sepD* strains with allelic replacements of *cesT* with *cesT1* and *cesT2* alleles display altered secretion profiles. (A) Total secreted proteins from the indicated strains were isolated and subjected to SDS-PAGE and Coomassie blue staining. Note the reduction of Tir and NleA for the Δ*sepD cesT1* and Δ*sepD cesT2* strains (indicated by arrowheads). EspC is secreted using the type 5 secretion pathway and is not affected. A Bradford assay was used to determine total protein amounts in the respective culture supernatants (bottom). (B) Total secreted proteins and cell lysates were collected and subjected to immunoblotting with the indicated antibodies. Densitometry was performed on the boxed signals for the Δ*sepD* strain and then used to normalize the corresponding signals from the other strains. The normalized values are shown below the blot images. Immunoblotting of whole-cell lysates was performed to assess cellular protein expression levels after 6 h, with the exception of NleA expression, which was measured after 3 h, which helped to reduce background signal levels typically observed in 6-h lysates (see, e.g., Fig. 2C). RNA polymerase is expected to be unchanged and represents a loading control. EscJ is a ring-forming protein of the T3SS apparatus and was detected to assess expression of the T3SS basal body within each sample. This experiment was performed at least three times, with representative data being shown.

dimerization (Fig. 4A) (see Fig. S3 in the supplemental material for additional structural correlation models). In the case of residue E68, it is surface exposed, and hence a replacement by a hydrophobic valine is predicted to disrupt interactions with other T3SS or effector proteins. The change of E68 to valine altered the hydrodynamic properties of soluble CesT in native PAGE compared to those of normal CesT (Fig. 4B, lower band in gel). Serine 119 localizes to the middle of helix α3 and a replacement by proline is predicted to disrupt secondary structure. With respect to intramolecular interactions, it is worth noting that the gamma hydroxyl group of serine 119 is in very close proximity to the gamma CH_2 of proline 82 and the aromatic moiety of phenylalanine 76, such that there is no clear need to satisfy an H bond with this serine (a feature that would be disrupted by the proline substitution). CesT(S119P) displayed slower migration in SDS-PAGE (Fig. 2A and Fig. 4C) [EPEC and BL21(λDE3) lysates, respectively] and was likely insoluble since almost no CesT(S119P) was detected in BL21(λDE3) soluble fractions (Fig. 4B).

Amino acid substitutions at H128R and H128Y were identified from the CesT variant library by producing reduced effector secretion levels. H128 is positioned at the end of a well-resolved helical structure (Fig. 4A) and could interact with other proteins. There is a potential for H128 to be involved in a putative stabilizing "ring" stacking interaction with Y124 (located within 6 Å) in wild-type CesT, although H128R and H128Y would both be able to participate in such an interaction. A Δ*sepD* Δ*cesT* strain expressing plasmid-encoded CesT(H128R) supported normal intracellular levels of Tir, yet NleA was not detectable within cell lysates (Fig. 2C). CesT(H128R) supported reduced secreted Tir levels, whereas NleA secretion was not apparent (as detected by immunoblotting analyses) (Fig. 2F). A Δ*sepD* Δ*cesT* strain expressing CesT(H128Y) exhibited normal intracellular Tir levels, and NleA was absent. With respect to secreted protein levels, CesT(H128Y) supported reduced and altered Tir secretion, with an appearance of novel degradation products detected with the anti-Tir antibodies (these were absent from the Δ*sepD* Δ*cesT*/pCesT strain). Furthermore, and in contrast to CesT(H128R), secreted NleA was detectable when the Δ*sepD* Δ*cesT* strain expressed CesT(H128Y), although only a lower-molecular-mass form was detected with anti-NleA antisera.

The immediately adjacent N129S substitution (isolated from the screen) results in a less bulky side group, which may alter interactions with other proteins since N129 is likely surface exposed based upon the position of H128 at the end of the resolved α3 helix.

Two isolates with substitutions at S147 were identified. CesT(S147G) and CesT(K108E,S147G) demonstrated a differential effector secretion profile, with reduced Tir levels and no NleA. We investigated the C-terminal region surrounding S147 by deleting the last 11 amino acids of CesT (Δ145-156). This truncated

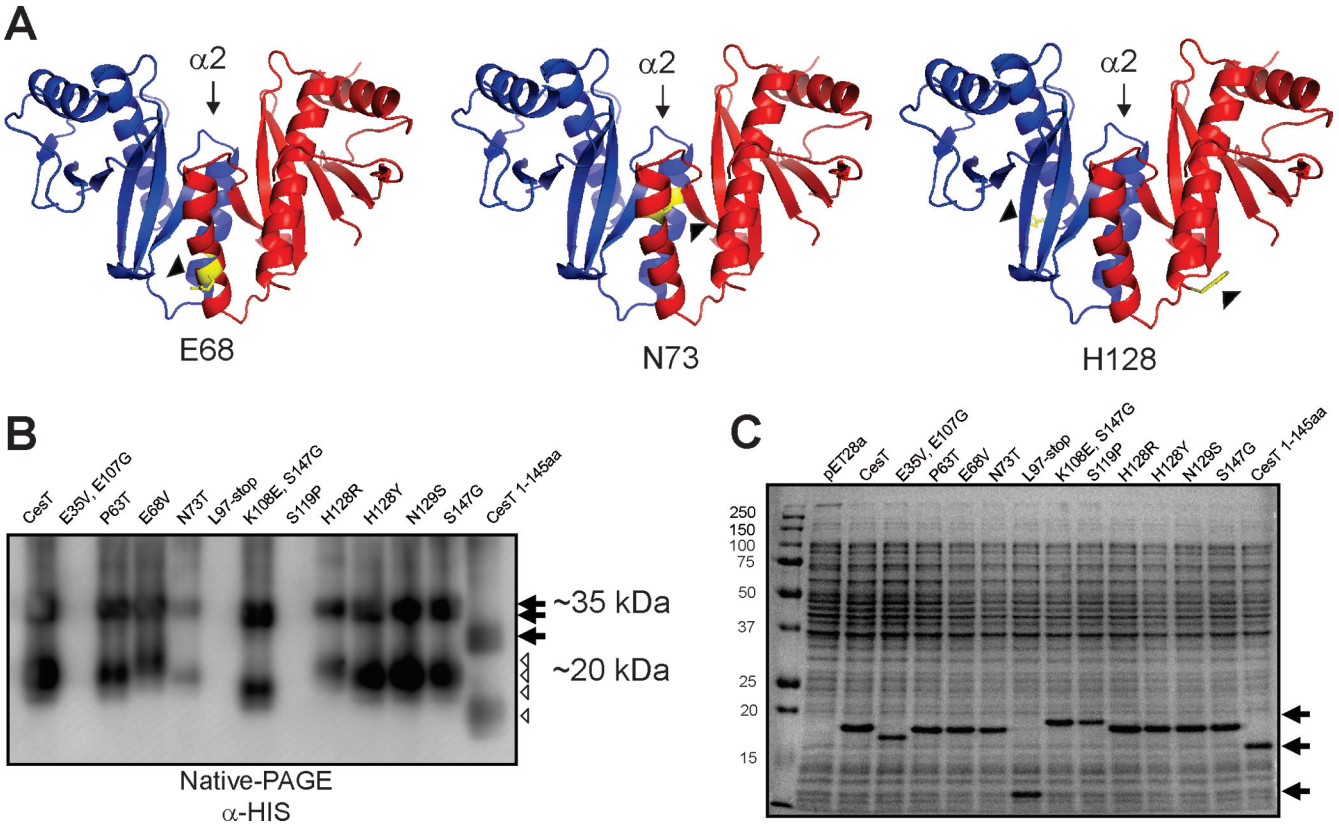

FIG 4 Structural modeling and biochemical characterization of CesT variants. (A) Structure-function correlation of CesT variants with altered surface-exposed amino acids predicted to be involved in effector interaction or type III secretion events. (B) Nondenaturing native protein gel electrophoresis of soluble protein preparations derived from IPTG-induced BL21(λDE3) cells overexpressing CesT variants. Anti-His antibodies detected putative dimeric (filled arrowheads) and monomeric (open arrowheads) CesT species. Native protein markers were used to determine migration distance during electrophoresis, with relevant sizes indicated adjacent to the blot. Note the altered migration pattern for certain CesT variants compared to wild-type CesT. (C) Overexpression of CesT variants in *E. coli* BL21(λDE3). Bacterial cultures were harvested after induction with 1 mM IPTG for 2 h. Whole-cell lysates were separated by SDS-PAGE and stained with Coomassie blue G-250. The arrows indicate altered migration patterns for certain CesT variants compared to wild-type CesT.

CesT variant was also shown to have a differential effector secretion profile, similar to that for S147G (a reduced Tir level and absent NleA) (Fig. 2D, E, and F). In summary, amino acids H128, N129, and S147 and the C-terminal 11 amino acids of CesT are implicated in CesT function with respect to effector secretion. CesT variants with amino acid substitutions within the α2 dimerization interface exhibited marked reductions in both Tir and NleA steady-state intracellular levels. NleA steady-state levels were reduced or completely absent for all CesT variants evaluated.

Soluble CesT variants dimerize and bind effectors to various extents. Selected mutated *cesT* alleles were cloned into a T7 promoter expression plasmid (pET28) to produce amino-terminal histidine-tagged CesT variants in *E. coli* BL21(λDE3). All of the CesT variants were expressed at levels comparable to that of His-CesT (Fig. 4C). Notably, some variants displayed slower migration patterns in SDS-PAGE, while one CesT variant (E35V/E107G) migrated faster. These findings are consistent with the pattern observed for CesT expression in the EPEC Δ*sepD* Δ*cesT* strain (Fig. 2A). Soluble fractions of the BL21(λDE3) lysates were prepared and subjected to nondenaturing (native) SDS-PAGE followed by immunoblotting with anti-His antibodies. Two protein species of approximately 35 kDa and 20 kDa were detected for CesT and most CesT variants (Fig. 4B). The higher-molecular-mass species is consistent with the previous observed formation of CesT dimers (8), whereas the lower mass is close to the predicted molecular mass of a CesT monomer (17.7 kDa). CesT(E35V/E107G) and CesT(S119P) were not detected to any extent in native protein gels. The putative CesT(E68V) and CesT(H128R) monomers were found to migrate slower than normal CesT within the native protein gel. CesT E68 is surface exposed, and therefore the loss of negative charge with a replacement by valine likely affected the CesT hydrodynamic properties and hence migration within the gel. CesT H128 is also surface exposed, and the replacement by arginine [CesT(H128R)] results in a positively charged side group with a pK_a of 12. This change is expected to alter its migration within the gel. Notably, a variant at the same position [CesT(H128Y)] migrated similarly to wild-type monomeric CesT, presumably due to no change in charge. Lastly, the CesT(K108E/S147G) variant monomer migrated faster in the native gel. This observation may be due to the replacement of lysine 108 by glutamic acid, since the variant with a single replacement of serine 147 by glycine behaved similarly to wild-type CesT. These native (nondenaturing) electrophoretic analyses indicate that most of the CesT variants can form stable dimers and have hydrodynamic properties similar to those of normal CesT.

DSF analyses of CesT and CesT variants. The inherent stabilities of Ni-NTA affinity-column purified His-CesT and His-CesT variants were assessed by differential scanning fluorimetry (DSF)

studies. DSF is an accepted spectroscopic technique that monitors thermal unfolding of proteins in the presence of a fluorescent dye. As a protein unfolds with an increase in temperature, the fluorescent dye binds to newly exposed hydrophobic amino acids and emits light at a defined wavelength. It is considered a reliable method to assess protein stability (56). Some CesT variants were recalcitrant to purification under soluble conditions, so we focused our efforts on the soluble CesT variants.

DSF analysis of purified CesT produced a spectroscopic fluorescence curve with an experimentally derived melting temperature (T_m) of 62.8°C (Fig. 5). Similar and overlapping fluorescence curves were obtained for CesT variants H128R, N129S, and S147G, with T_m values ranging from 62.3 to 62.8°C. CesT(H128Y) had higher fluorescence emission at lower temperature, although as temperature increased, fluorescence emission was similar to that of CesT (see Discussion). In stark contrast, CesT variants P63T, E68V, and K108/S147G produced dramatically shifted curves and lower T_m values, ranging from 55 to 56°C. These three less stable CesT variants were deliberately included in the DSF assay, as we predicted them to be less stable due to mutations in the CesT α2 dimerization interface. To assess the validity of our experimental approach, we assayed purified hen egg lysozyme as a model protein substrate. A characteristic curve similar to that previously reported was obtained (56), with a experimentally determined T_m of 73.8°C. This value equals the T_m for hen egg lysozyme as determined by circular dichroism analysis (57). These DSF assays indicate that C-terminal CesT variants H128R, N129S, and S147G exhibit protein stability similar to that of normal CesT. Destabilized CesT variants exhibited lower T_m values than normal CesT.

C-terminal CesT variants bind effectors similarly to wild-type CesT. The native PAGE experiments and DSF analyses indicated similar hydrodynamic and stability properties for CesT and C-terminal CesT variants. To further assess CesT variant dimer function, we set out to evaluate the ability of certain CesT variants to bind effectors. In our hands, purifying stable, intact, and soluble forms of Tir or NleA (in the absence of CesT) continues to be experimentally challenging. Nonetheless, we have previously shown that purified His-CesT can "capture" multiple EPEC effectors derived from culture supernatants in an *in vitro* CesT affinity column binding assay (4). We focused our attention on CesT C-terminal variants [H128R, H128Y, N129S, S147G, and CesT(Δ145-156)], as these constructs exhibited near-normal intracellular levels of Tir within EPEC and retained dimer formation (Fig. 2B and 4B), two observations consistent with Tir binding and stability. Therefore, normal (wild-type) CesT and these CesT variants were overexpressed and purified from BL21(λDE3) lysates using Ni-NTA column chromatography and used in an effector binding assay. Purified CesT efficiently bound and retained multiple protein species from a Δ*sepD* culture supernatant as indicated by the absence of specific protein species from column flowthrough fraction (Fig. 6A). Notably, most EspC protein was not retained and was found within the flowthrough fraction, thus demonstrating CesT affinity column binding for type III secreted effectors, confirming previous results (39). The CesT(H128R), CesT(N129S), CesT(S147G), and CesT(Δ145-156) flowthrough fractions appeared similar to that for CesT. In contrast, the CesT(H128Y) flowthrough fraction contained small amounts of protein species with molecular masses similar to those found in the Δ*sepD* precolumn supernatant, in addition to a novel 10-kDa species. After extensive washing, each of the columns was treated with imidazole to coelute the bound proteins along with His-CesT or His-CesT variant. SDS-PAGE analysis revealed that all of the elution profiles appeared similar by Coomassie blue staining (Fig. 6B). For unknown reasons, the His-CesT(Δ145-156) variant was less abundant than the other CesT variants, although it was still able to retain effector proteins. Immunoblotting the elution fractions with anti-Tir and anti-NleA antibodies revealed that equivalent levels of these effectors were eluted from the respective columns (Fig. 6B). Similar results were obtained when reduced amounts of His-CesT or His-CesT variants were exposed to excess amounts of effector proteins (data not shown). These data indicate that CesT C-terminal variants H128R, N129S, S147G, and Δ145-156 bind effectors similarly to normal CesT. CesT(H128Y) was less efficient at initial binding of effectors but was able to retain effectors similarly to normal CesT. As shown above (Fig. 2E), CesT(H128Y) expression within the Δ*sepD* Δ*cesT* strain resulted in reduced intact Tir secretion levels and the appearance of novel Tir species in culture supernatants (see discussion).

Alanine, threonine, and glutamic acid scanning mutagenesis identifies two C-terminal serine residues as important factors in supporting proper CesT functionality. It has been demonstrated that hierarchical Tir translocation occurs during *in vitro* EPEC infection and that the observed hierarchy is dependent on CesT (37, 39). Furthermore, a previously characterized CesT(E142G) variant is known to bind Tir but supports reduced Tir secretion. As structural data for the C-terminal region of CesT (amino acids 145 to 156) are lacking and in light of our secretion screen results, we set out to further characterize this region using site-directed mutagenesis. The CesT S147G variant (from the error-prone library) formed the rationale for our mutagenesis approach. Polyserine regions within proteins are known to provide flexibility. We therefore targeted three adjacent serine residues, S145, S146, and S147, for alanine, threonine, and glutamic acid scanning mutagenesis. The rationale was that alanine substitution would not induce any major structural changes and would likely reproduce the CesT(S147G) phenotype. Threonine substitution would be a conservative change owing to polar features and the presence of a hydroxyl side group similar to serine, and lastly, glutamic acid substitution would represent a dramatic change introducing a large, negatively charged amino acid.

Nine CesT variants were generated (Table 2) and then introduced into the Δ*sepD* Δ*cesT* strain for phenotypic characterization. Immunoblotting analysis of the CesT variants demonstrated expression levels equivalent to that of natively expressed CesT in the Δ*sepD* strain (Fig. 7A). Secreted protein fractions were collected, subjected to SDS-PAGE, and stained with Coomassie blue G-250. Replacement of serine 145 by alanine, threonine, or glutamic acid did not have any apparent effect on the secretion profile compared to that of the Δ*sepD* Δ*cesT* strain expressing wild-type CesT, although a slight reduction in the amount of total secreted protein was evident (Fig. 7B). In contrast, replacement of serine 146 by alanine, threonine, or glutamic acid resulted in a notable decrease in secreted NleA (Fig. 7A). Replacement of serine 147 by alanine or glutamic acid strongly reduced NleA secretion, whereas threonine substitution resulted in only a modest decrease in secreted NleA levels. In agreement, a Δ*sepD cesT1* strain expressing CesT(S147A) from the normal *cesT* allele chromosomal location (*cis*-complementation) exhibited the same secretion profile (shown in Fig. 3B) as the *trans*-complemented strain (Fig. 7A).

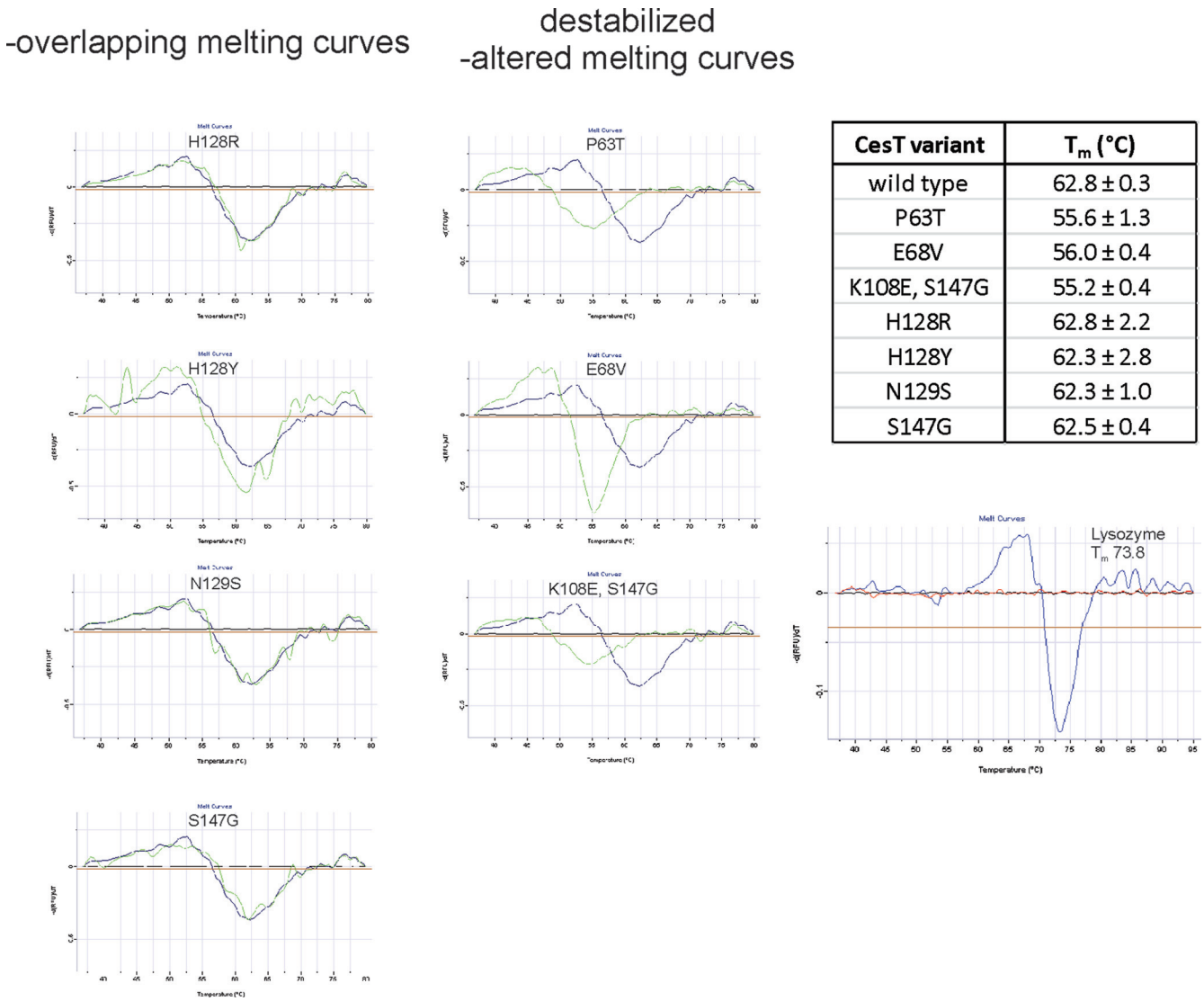

CesT variant	T_m (°C)
wild type	62.8 ± 0.3
P63T	55.6 ± 1.3
E68V	56.0 ± 0.4
K108E, S147G	55.2 ± 0.4
H128R	62.8 ± 2.2
H128Y	62.3 ± 2.8
N129S	62.3 ± 1.0
S147G	62.5 ± 0.4

FIG 5 Differential scanning fluorimetry (DSF) analyses of purified CesT and CesT variants. Melt curves were plotted as a function of the first derivative of relative fluorescence (*y* axis) versus temperature (°C) (*x* axis). The blue line in each plot depicts thermal denaturation of normal CesT compared to that of a specific CesT variant (green line). Plots in the left column overlap, indicative of similar protein stability to normal CesT. Plots in the right column demonstrate shifted curves, indicative of different (altered) protein stability than normal CesT. The inset table shows an average of the experimentally derived melting temperature (T_m) for each protein ($n = 2$). Hen egg lysozyme was used as a model protein to assess the experimental protocol and accuracy (bottom right plot, blue line). Red and black lines represent controls for Sypro orange (only) and lysozyme (only), respectively. The experimentally determined T_m value for lysozyme using this approach was consistent with the reported literature. This experiment was performed twice. Representative melting curves are shown.

Furthermore, using anti-NleA antibodies, immunoblots of the *cis*-complemented CesT(S147A)-expressing strain revealed markedly reduced NleA secreted levels compared to those for the Δ*sepD* strain (Fig. 3B). For all substitutions, Tir secretion levels did not change to any significant extent as determined by band intensity in Coomassie blue-stained gels. The secreted protein fractions were quantified for total protein amount using a Bradford assay. While all the CesT variants supported reduced total protein amounts, the largest reductions were apparent for CesT variants with substitutions at serine 146 and serine 147 (Fig. 7B). To summarize the site-directed mutagenesis data, CesT serines 146 and 147 contributed to efficient effector secretion, a result that corroborates the deficiency of the CesT(S147G) variant identified from the error-prone PCR CesT expression library (Fig. 2D, E, and F). Serine 146 had a modest role in effector secretion, whereas serine 145 had a minor role.

The C-terminal region of CesT is important for maximal NleA but not Tir translocation into host cells during infection. To investigate the ability of CesT variants to direct effector translocation into host cells, an infection assay was carried out to evaluate translocation of the EPEC effectors Tir and NleA into host cells. Initially we screened all the plasmid-expressed CesT variants for their ability to restore Tir-mediated actin pedestal formation to a *cesT* null mutant. These data demonstrated reduced actin pedestal formation to various extents in all cases (Fig. 8A). Notably, C-terminal CesT variants H128Y, H128R, and N129S all demonstrated significantly lower numbers of actin pedestals than wild-type CesT (approximately 45 to 60%). Bacteria expressing CesT(S147G) supported

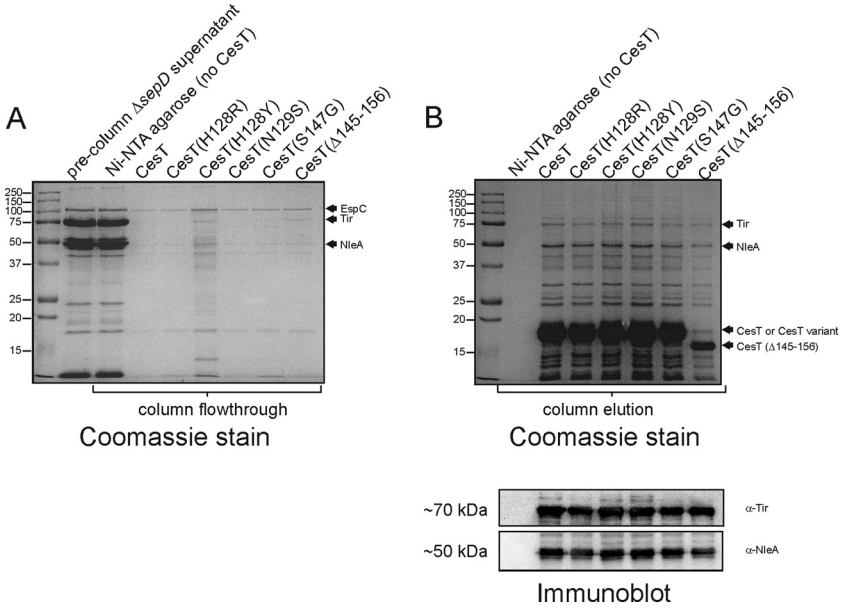

FIG 6 Purified, nickel column-bound His-CesT variants bind secreted effectors from culture supernatants. (A) Equal amounts of a Δ*sepD* Δ*cesT* culture supernatant preparation were passed through nickel resin columns containing His-CesT variants (or an empty column with nickel resin), and the flowthrough fractions were examined by SDS-PAGE and Coomassie blue staining. The identities of EspC, Tir, and NleA (arrows) have been previously determined by mass spectrometry analyses. (B) The imidazole elution fractions of the "captured" proteins along with respective His-CesT variants were evaluated by SDS-PAGE and Coomassie blue staining and by immunoblotting with the indicated antibodies.

modestly reduced actin pedestal formation (89% ± 6%) compared to those expressing CesT (Fig. 8A). As expected, bacteria expressing CesT(S147A) were found to support pedestal formation similarly to bacteria expressing CesT(S147G) (data not shown).

To investigate if CesT has specific roles for other type III effectors, we evaluated NleA, mainly due to our observation that NleA secretion was absent or reduced for most CesT variants (Fig. 2F). Upon infection, NleA has been shown to localize to the Golgi

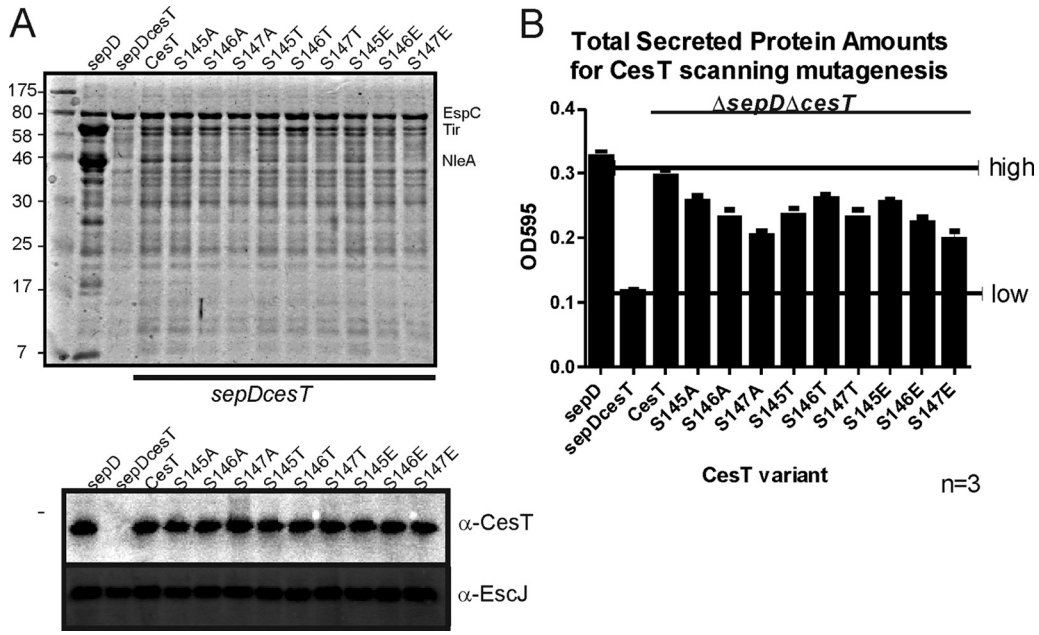

FIG 7 CesT variants at a triple-serine motif have reduced total effector secretion levels. (A) Top, total secreted proteins collected from culture supernatants of the various bacterial strains separated by SDS-PAGE and stained with Coomassie blue. Note the reduction of protein species in the *sepD cesT* double mutant and the restoration of proteins with CesT. The S147A variant appears to secrete Tir but not NleA and validates the S147G library isolate. EspC is a type V secreted protein that is not dependent on CesT and therefore serves as a loading control for each supernatant sample. Bottom, bacterial whole-cell lysates were probed with the indicated antibodies to assess protein expression. EscJ is an inner ring component of the T3SS (not dependent on CesT) and served to indicate equal needle expression among samples. (B) Quantification of total secreted proteins using a Bradford assay. The high and low horizontal bars represent the levels of pCesT complementation and Δ*sepD* Δ*cesT*, respectively.

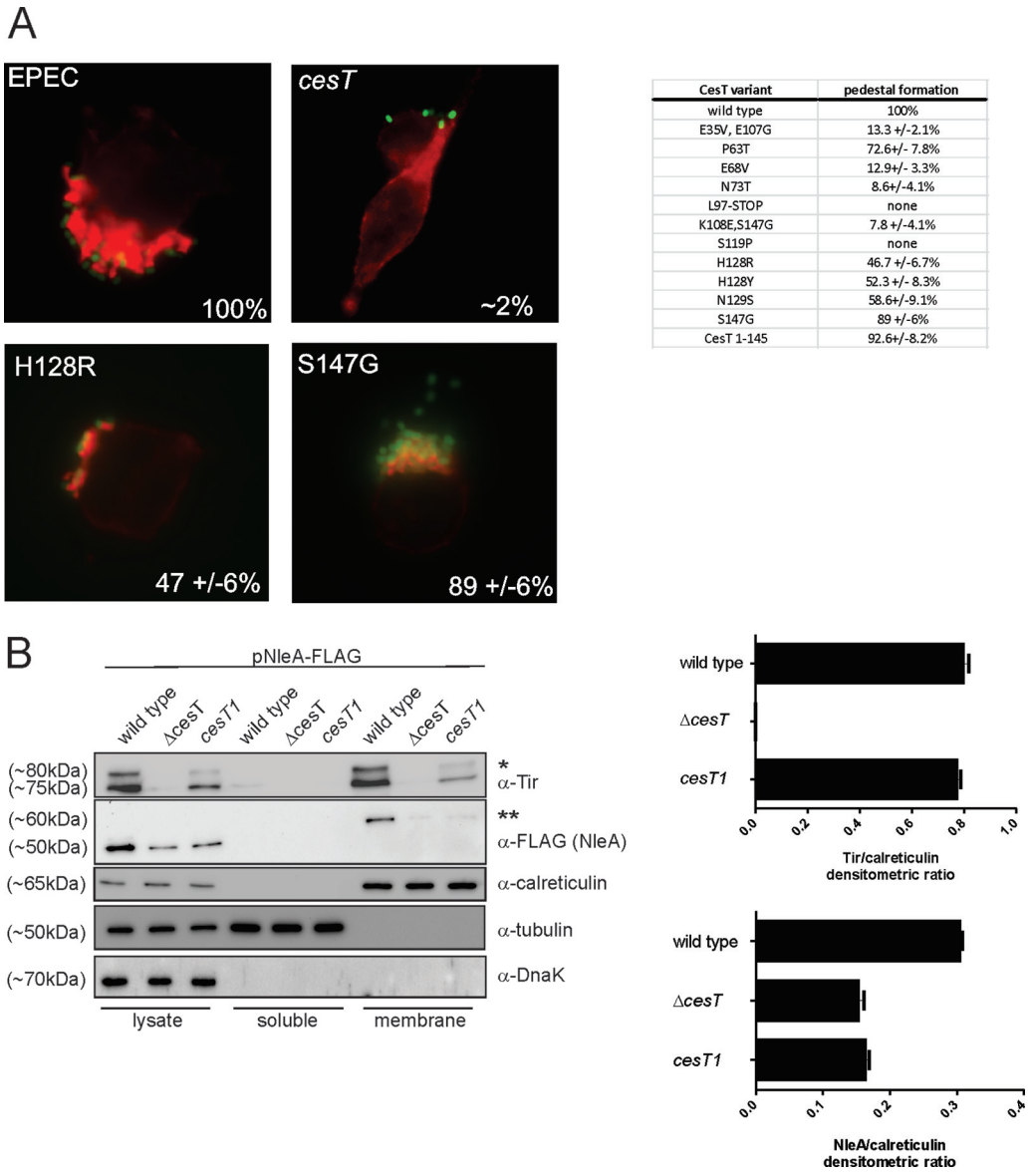

CesT variant	pedestal formation
wild type	100%
E35V, E107G	13.3 +/-2.1%
P63T	72.6+/- 7.8%
E68V	12.9+/- 3.3%
N73T	8.6+/-4.1%
L97-STOP	none
K108E,S147G	7.8 +/-4.1%
S119P	none
H128R	46.7 +/-6.7%
H128Y	52.3 +/- 8.3%
N129S	58.6+/-9.1%
S147G	89 +/-6%
CesT 1-145	92.6+/-8.2%

FIG 8 Infection of HeLa cells with wild-type or Δ*cesT* mutant EPEC expressing CesT variants. (A) Fluorescence microscopy to detect Tir-mediated F-actin pedestal formation. The infected HeLa cells were washed, fixed, and stained with Alexa-568-conjugated phalloidin (red). The extracellular adherent bacteria express green fluorescent protein (GFP) and therefore appear green. Note the focusing of filamentous actin underneath adherent wild-type EPEC and the Δ*cesT*/pCesT(H128R) and Δ*cesT*/pCesT(S147G) mutants but not the *cesT* null mutant. The table (right) shows data for other CesT variants. The indicated percentages are averages (with standard deviations) derived by enumerating actin pedestals from three independent experiments. (B) HeLa cells were infected with the indicated strains, followed by mechanical fractionation to produce crude lysates and soluble and membrane fractions. The fractions were separated by 10% SDS-PAGE and immunoblotted with the indicated antibodies. Calreticulin is a eukaryotic membrane protein that served as membrane indicator for the fractionation procedure and to perform normalized densitometry analyses for translocated Tir and NleA levels (single and double asterisks, respectively) as determined by ImageLab software (shown as a ratio in the bar graph at the right). This experiment was performed three times. Representative images of immunoblots are shown.

apparatus, where it is thought to disrupt protein trafficking through COPII-dependent pathways (58). NleA strictly requires a functional T3SS for translocation into host cells (48) and is known to interact with CesT (4) (Fig. 6B). Moreover, CesT is not required for *nleA* gene transcription (39). We therefore set out to measure levels of NleA translocation into host cells. Unfortunately, our anti-NleA polyclonal rat antibody was not able to detect native NleA levels during infection. For these experiments, we generated strains harboring plasmids expressing epitope-tagged NleA (NleA-FLAG) expressed from the *nleA* transcriptional promoter. We were unable to use CesT variants expressed from plasmids as the combination of both NleA- and CesT-expressing plasmids reduced the efficiency of EPEC infection of HeLa cells. We therefore generated a strain expressing CesT(S147A) by replacing the normal *cesT* gene on the chromosome with a corresponding mutated *cesT* gene, and we named this the *cesT1* strain. The rationale to generate a *cesT1* strain expressing CesT(S147A) was due to our previous observation that plasmid-encoded CesT(S147A) sup-

ported Tir secretion and reduced NleA secretion for a Δ*sepD* Δ*cesT* mutant (Fig. 7). The *cesT1* strain expressed amounts of EspA, EspB, and EspD (filament and pore-forming proteins) comparable to those expressed by wild-type EPEC (see Fig. S4 in the supplemental material). Importantly, and as expected, the CesT(S147A) variant protein was expressed at levels equal to those of native CesT. These data therefore validate the use of *cesT1* strain for CesT(S147A)-related observations. Infected HeLa monolayers were then infected with EPEC Δ*cesT* and *cesT1* strains expressing NleA-FLAG, followed by fractionation of the infected HeLa cells to detect Tir and NleA translocation levels by immunoblotting. Both the wild-type and *cesT1* strains translocated Tir into HeLa cells, as shown by the detection of this effector in the HeLa membrane fraction (Fig. 8B). In contrast, Δ*cesT* did not demonstrate Tir translocation, confirming previous results (21). The wild type translocated NleA-FLAG into the HeLa cell membrane fraction, whereas the Δ*cesT* and *cesT1* strains both translocated significantly reduced levels of NleA-FLAG compared to wild type as determined by quantitative densitometry of immunoblot signals. We did note that intracellular (bacterium-associated) NleA-FLAG steady-state levels were reduced for the Δ*cesT* and *cesT1* strains, although normalization for expression amounts within each strain still revealed lower NleA-FLAG translocation levels.

DISCUSSION

Multicargo chaperones are known to bind different effectors, a process that contributes to pathogenesis, although few studies have investigated how these chaperones coordinate intermolecular interactions and protein trafficking within the bacterial cell.

Previous studies with CesT identified surface-exposed hydrophobic amino acids and a coiled-coil domain as important determinants for substrate interactions (8, 40). For a relatively small protein, CesT exhibits many surface-exposed hydrophobic amino acids (8), and therefore it was predicted that those amino acids would be involved in binding interactions with partner proteins. In cases where chaperone-effector cocrystal structures or NMR studies are available, researchers have been guided toward rationale site-directed mutagenesis studies (59, 60). Unfortunately a CesT-effector cocrystal structure is not available to guide mutagenesis studies. Moreover, Tir is known to strictly require CesT binding for its intracellular stability, so Tir amino acid variants (mutagenesis studies) are often difficult to interpret. We therefore focused our efforts on CesT variants and developed a functional screen for CesT. It was discovered that the C-terminal region of CesT is involved in type III effector secretion. An important observation from this work is that CesT roles in effector binding and secretion are separable events and are likely controlled by different parts of the functional dimer.

CesT differs from other multicargo effector chaperones in that it is larger (156 amino acids). Using protein alignment tools, CesT has been shown to have an additional 20 to 25 amino acids at the C terminus (see Fig. S5 in the supplemental material). Based on alignment algorithms, CesT H128 and N129 are the exact amino acid positions corresponding to the C termini of Spa15 and InvB. Our functional screen resulted in the identification of three functionally deficient CesT variants at this exact location (H128R, H128Y, and N129S), which is indicative of important structural features for this part of the CesT dimer. Since Tir intracellular stability was not compromised for any of these CesT variants, this location may have a role in mediating an appropriate contact with an unidentified component of the T3SS. We found that CesT(H128Y) was less efficient in initial binding of effectors than normal CesT in an *in vitro* column assay (Fig. 5A). This finding is in agreement with the observation of an aberrant effector secretion profile for the Δ*sepD* Δ*cesT* strain expressing CesT(H128Y), which exhibited aberrant Tir-derived polypeptide species and less intact Tir (Fig. 2D). While we do not know the exact mechanism behind this observation, we do know that purified CesT(H128Y) exhibited increased fluorescence at lower temperatures when analyzed by DSF (Fig. 5). This may be indicative of increased surface hydrophobicity due to a hydrophobic tyrosine replacing histidine (resulting in increased fluorescence in DSF), or it may suggest localized destabilization within CesT(H128Y) upon thermal denaturation.

The CesT C-terminal region is net positively charged (amino acids 148 to 156, DNKHYYAGR). We speculate that this region may be involved in interactions with other T3SS components. Helical wheel analysis did not demonstrate amphipathic properties within this region (data not shown); however, formation of a β-strand would provide a cationic face with the arginine and lysine side chains. It is has been proposed that large tyrosine residues are ideal for mediating molecular contacts and that small serine residues can provide flexibility to short or minimalist binding sites (61). Our CesT(Δ145-156) variant along with the triple-serine site-directed mutagenesis results, especially for CesTS147, are supportive of this view.

We noticed that the *trans*-complemented Δ*sepD* Δ*cesT* double mutant (with pCesT) did not return secretion to exactly Δ*sepD* levels. The pCesT plasmid employs the *lac* promoter to express *cesT*; therefore, native transcriptional regulatory mechanisms were not restored. For unknown reasons, we were unable to generate a plasmid with the *LEE5* promoter that would potentially support "native" *cesT* expression. Instead, we generated *cis*-complemented strains for *cesT1* and Δ*sepD cesT1*, both expressing CesT(S147A), and Δ*sepD cesT2*, expressing CesT(H128R). These *cis*-complemented strains exhibited the same secretion profile as the corresponding CesT variant plasmid *trans*-complemented strains. These data suggest that the plasmid *trans*-complementation system, while imperfect, was nonetheless reliable and informative with respect to CesT function.

Comparison of CesT sequences from various pathogenic *E. coli* strains (enterohemorrhagic *E. coli* [EHEC] and EPEC) indicates an overall high level of protein sequence identity (95 to 100%) (data not shown). Therefore, CesT is highly conserved, which suggests that CesT function is retained in various pathogenic attaching and effacing *E. coli* strains. One localized region of difference within CesT is at position 146, where serine is replaced by proline. This is observed in EPEC O157:H45 and EPEC RN587/1, two EPEC strains associated with diarrheal illness. Interestingly, this discrete region of CesT was identified in our mutagenesis screen as being important in supporting effector secretion. We speculate that a structural turn imposed by proline at position 146 serves to present the C-terminal region (aa 147 to 156) to appropriate binding surfaces.

This study reports on the contribution of the C-terminal region of CesT in effector secretion, which is a first for the family of multicargo type III secretion chaperones. The only instance in the literature of a similar observation is found for the related flagellar type III export pathway, where the FlgN chaperone is known to contribute to secretion of the hook filament proteins FlgK and

FlgL (62). FlgN has been demonstrated to interact with the ATPase FliI and also with the C-terminal region of FlhA (an export apparatus component) (3, 63). Recently, a highly conserved FlgN C-terminal tyrosine residue (Y122) has been implicated in an interaction with FlhA (63). It is tempting to speculate that a similar protein interaction paradigm applies to EPEC CesT with EscV (FlhA homologue), a question that we will attempt to address in future studies.

It has been demonstrated by several research groups that Tir translocation appears to be a hierarchical process (37, 39, 47), occurring before other effectors are injected into host cells. Our data indicate Tir secretion even with alteration of CesT at the C-terminal region, whereas in stark contrast, NleA secretion was impaired with CesT alteration. Other EPEC effectors have been shown to be translocated into host cells at reduced levels in the absence of CesT (64, 65), indicating that CesT contributes to fully competent effector translocation. With respect to effector translocation order, the current data cannot discern the reason for the apparent preference for Tir over other effectors, although we speculate that Tir may have a high affinity for CesT that promotes its hierarchical translocation order. We have been unable to overexpress and purify intact Tir or NleA effector proteins in the absence of overexpressed CesT, an issue that has prevented us from performing appropriate affinity binding studies.

Based on literature from T3SS studies and our own experimental findings, we present hypothetical models depicting CesT in effector trafficking events (Fig. 9). The needle complex and core export apparatus of the T3SS along with a hexameric ATPase are all required for effector protein secretion and are therefore present in each model. Furthermore, an N-terminal secretion signal is present on effector proteins and has been shown to interact with the T3SS ATPase (66). CesT-effector complexes have been demonstrated to interact with membranes in the absence of EscN (4), and hence we also present a model where an initial interaction with the membrane occurs, followed by a secondary "on-off" interaction with EscN, to deliver the effector to the T3SS. It is debatable whether T3SS ATPases are stable components of the core T3SS apparatus, as these ATPases have been detected in cytoplasmic fractions but also have a high affinity for membranes (4, 67). Therefore, another possible model is the formation of an initial tripartite ATPase-chaperone-effector complex. Such complexes have been identified in partially reconstituted *in vitro* systems (2, 68). The ATPase-chaperone-effector complex could interact with the inner membrane and then engage the core export apparatus. Importantly, stable YscLNQ and EscLNQ protein complexes have been reported (69, 70), and therefore all models converge on EscN (ATPase) engagement at the base of the T3SS export apparatus. The ATPase is then postulated to dissociate the chaperone-effector complex and further unfold the effector protein to allow entry into the base of the T3SS (2). Additional studies are required to refine these models, although we envision that certain effectors might have intrinsic features that contribute to differential secretion efficiencies. These may include cotranscriptional regulation, higher binding affinities, or ordered interactions with key T3SS components and effector stability. There is compelling experimental evidence for each of the models, suggesting that cooperative protein interactions sequentially occur with T3SS components to mediate type III secretion.

In summary, this study presents findings that highlight several roles for the multicargo T3SC CesT. CesT dimerization was demonstrated to be important for its role in stabilizing effectors. Moreover, specific regions of CesT were shown to not be involved in stabilizing events but rather were involved in promoting efficient effector secretion. Lastly, genetic and biochemical approaches provide data that implicate the positively charged C-terminal region of CesT in secretion events. These structure/function findings should be valuable in future studies to discover potential T3SC inhibitor molecules, a strategy that could reduce the disease burden caused by pathogens using the T3SS during infection.

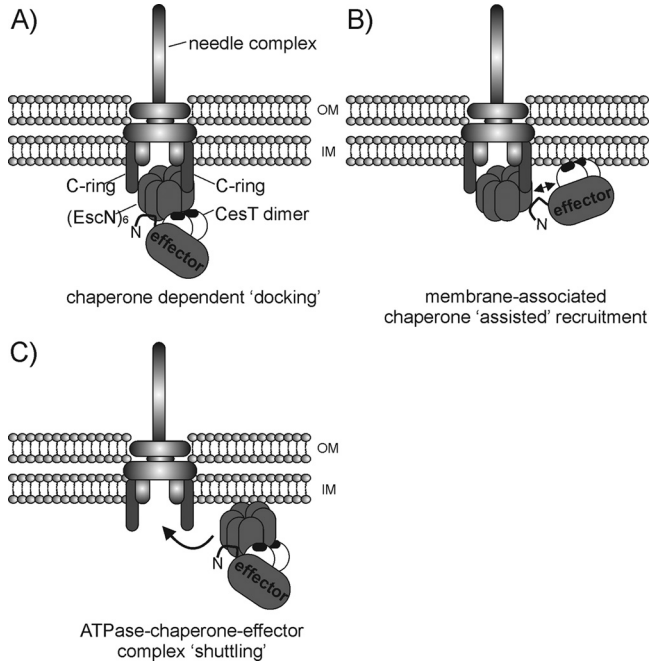

FIG 9 Hypothetical models of type III effector targeting to the base of the bacterial T3SS. (A) Chaperone-dependent docking of an effector with the hexameric T3SS ATPase (EscN). The C-terminal region of CesT is shaded black to indicate the importance of this region in docking events. In this case, CesT provides stability and docking roles. An N-terminal secretion signal on the effector is known to interact with the hexameric T3SS ATPase (62). (B) CesT-effector complexes may interact with the inner membrane or with unidentified membrane-associated components, followed by an EscN interaction. This model is supported by observations of CesT-effector complexes associating with membranes in the absence of EscN (68). Uncomplexed CesT may remain at the membrane to bind additional effector cargo, serving as a localized adaptor to facilitate effector secretion. (C) Tripartite ATPase-chaperone-effector complexes may form at the membrane, followed by a shuttling mechanism. Evidence for this model comes from *in vitro re*constitution experiments (2).

ACKNOWLEDGMENTS

We thank members of the Thomas lab and colleagues for critical reading of the manuscript. We thank Samantha Gruenheid for the kind gift of anti-NleA antibodies.

This work was supported by the Canadian Institutes of Health Research (CIHR, MOP84472), the Dalhousie Medical Research Foundation, and an infrastructure grant from the Canadian Foundation for Innovation (Leaders Opportunity Fund). N.A.T. is the recipient of a CIHR/Nova Scotia Health Research Foundation New Investigator Award.

REFERENCES

1. **Buttner D.** 2012. Protein export according to schedule: architecture, assembly, and regulation of type III secretion systems from plant- and animal-pathogenic bacteria. Microbiol. Mol. Biol. Rev. **76**:262–310.

2. **Akeda Y, Galan JE.** 2005. Chaperone release and unfolding of substrates in type III secretion. Nature **437**:911–915.
3. **Thomas J, Stafford GP, Hughes C.** 2004. Docking of cytosolic chaperone-substrate complexes at the membrane ATPase during flagellar type III protein export. Proc. Natl. Acad. Sci. U. S. A. **101**:3945–3950.
4. **Thomas NA, Deng W, Puente JL, Frey EA, Yip CK, Strynadka NC, Finlay BB.** 2005. CesT is a multi-effector chaperone and recruitment factor required for the efficient type III secretion of both LEE- and non-LEE-encoded effectors of enteropathogenic *Escherichia coli*. Mol. Microbiol. **57**:1762–1779.
5. **Quinaud M, Chabert J, Faudry E, Neumann E, Lemaire D, Pastor A, Elsen S, Dessen A, Attree I.** 2005. The PscE-PscF-PscG complex controls type III secretion needle biogenesis in *Pseudomonas aeruginosa*. J. Biol. Chem. **280**:36293–36300.
6. **Faudry E, Job V, Dessen A, Attree I, Forge V.** 2007. Type III secretion system translocator has a molten globule conformation both in its free and chaperone-bound forms. FEBS J. **274**:3601–3610.
7. **Page AL, Parsot C.** 2002. Chaperones of the type III secretion pathway: jacks of all trades. Mol. Microbiol. **46**:1–11.
8. **Luo Y, Bertero MG, Frey EA, Pfuetzner RA, Wenk MR, Creagh L, Marcus SL, Lim D, Sicheri F, Kay C, Haynes C, Finlay BB, Strynadka NC.** 2001. Structural and biochemical characterization of the type III secretion chaperones CesT and SigE. Nat. Struct. Biol. **8**:1031–1036.
9. **Birtalan S, Ghosh P.** 2001. Structure of the *Yersinia* type III secretory system chaperone SycE. Nat. Struct. Biol. **8**:974–978.
10. **Faherty CS, Maurelli AT.** 2009. Spa15 of *Shigella flexneri* is secreted through the type III secretion system and prevents staurosporine-induced apoptosis. Infect. Immun. **77**:5281–5290.
11. **Forsberg A, Wolf-Watz H.** 1990. Genetic analysis of the *yopE* region of *Yersinia* spp.: identification of a novel conserved locus, *yerA*, regulating *yopE* expression. J. Bacteriol. **172**:1547–1555.
12. **Ghosh P.** 2004. Process of protein transport by the type III secretion system. Microbiol. Mol. Biol. Rev. **68**:771–795.
13. **Thomas NA, Ma I, Prasad ME, Rafuse C.** 2012. Expanded roles for multicargo and class 1B effector chaperones in type III secretion. J. Bacteriol. **194**:3767–3773.
14. **Creasey EA, Delahay RM, Bishop AA, Shaw RK, Kenny B, Knutton S, Frankel G.** 2003. CesT is a bivalent enteropathogenic *Escherichia coli* chaperone required for translocation of both Tir and Map. Mol. Microbiol. **47**:209–221.
15. **Bronstein PA, Miao EA, Miller SI.** 2000. InvB is a type III secretion chaperone specific for SspA. J. Bacteriol. **182**:6638–6644.
16. **Lee SH, Galan JE.** 2003. InvB is a type III secretion-associated chaperone for the *Salmonella* enterica effector protein SopE. J. Bacteriol. **185**:7279–7284.
17. **Ehrbar K, Friebel A, Miller SI, Hardt WD.** 2003. Role of the *Salmonella* pathogenicity island 1 (SPI-1) protein InvB in type III secretion of SopE and SopE2, two *Salmonella* effector proteins encoded outside of SPI-1. J. Bacteriol. **185**:6950–6967.
18. **Page AL, Sansonetti P, Parsot C.** 2002. Spa15 of *Shigella flexneri*, a third type of chaperone in the type III secretion pathway. Mol. Microbiol. **43**:1533–1542.
19. **Cooper CA, Zhang K, Andres SN, Fang Y, Kaniuk NA, Hannemann M, Brumell JH, Foster LJ, Junop MS, Coombes BK.** 2010. Structural and biochemical characterization of SrcA, a multi-cargo type III secretion chaperone in *Salmonella* required for pathogenic association with a host. PLoS Pathog. **6**:e1000751. doi:10.1371/journal.ppat.1000751.
20. **Spaeth KE, Chen YS, Valdivia RH.** 2009. The *Chlamydia* type III secretion system C-ring engages a chaperone-effector protein complex. PLoS Pathog. **5**:e1000579. doi:10.1371/journal.ppat.1000579.
21. **Abe A, de Grado M, Pfuetzner RA, Sanchez-Sanmartin C, Devinney R, Puente JL, Strynadka NC, Finlay BB.** 1999. Enteropathogenic *Escherichia coli* translocated intimin receptor, Tir, requires a specific chaperone for stable secretion. Mol. Microbiol. **33**:1162–1175.
22. **Elliott SJ, Hutcheson SW, Dubois MS, Mellies JL, Wainwright LA, Batchelor M, Frankel G, Knutton S, Kaper JB.** 1999. Identification of CesT, a chaperone for the type III secretion of Tir in enteropathogenic *Escherichia coli*. Mol. Microbiol. **33**:1176–1189.
23. **Buttner D, Gurlebeck D, Noel LD, Bonas U.** 2004. HpaB from *Xanthomonas campestris pv. vesicatoria* acts as an exit control protein in type III-dependent protein secretion. Mol. Microbiol. **54**:755–768.
24. **Deng W, Puente JL, Gruenheid S, Li Y, Vallance BA, Vazquez A, Barba J, Ibarra JA, O'Donnell P, Metalnikov P, Ashman K, Lee S, Goode D, Pawson T, Finlay BB.** 2004. Dissecting virulence: systematic and functional analyses of a pathogenicity island. Proc. Natl. Acad. Sci. U. S. A. **101**:3597–3602.
25. **Darwin KH, Miller VL.** 2001. Type III secretion chaperone-dependent regulation: activation of virulence genes by SicA and InvF in *Salmonella typhimurium*. EMBO J. **20**:1850–1862.
26. **Tucker SC, Galan JE.** 2000. Complex function for SicA, a *Salmonella enterica* serovar Typhimurium type III secretion-associated chaperone. J. Bacteriol. **182**:2262–2268.
27. **Frithz-Lindsten E, Rosqvist R, Johansson L, Forsberg A.** 1995. The chaperone-like protein YerA of *Yersinia pseudotuberculosis* stabilizes YopE in the cytoplasm but is dispensible for targeting to the secretion loci. Mol. Microbiol. **16**:635–647.
28. **Wattiau P, Cornelis GR.** 1993. SycE, a chaperone-like protein of *Yersinia enterocolitica* involved in Ohe secretion of YopE. Mol. Microbiol. **8**:123–131.
29. **Lara-Tejero M, Kato J, Wagner S, Liu X, Galan JE.** 2011. A sorting platform determines the order of protein secretion in bacterial type III systems. Science **331**:1188–1191.
30. **Rodgers L, Gamez A, Riek R, Ghosh P.** 2008. The type III secretion chaperone SycE promotes a localized disorder-to-order transition in the natively unfolded effector YopE. J. Biol. Chem. **283**:20857–20863.
31. **Rodgers L, Mukerjea R, Birtalan S, Friedberg D, Ghosh P.** 2010. A solvent-exposed patch in chaperone-bound YopE is required for translocation by the type III secretion system. J. Bacteriol. **192**:3114–3122.
32. **Cheng LW, Schneewind O.** 1999. *Yersinia enterocolitica* type III secretion. On the role of SycE in targeting YopE into HeLa cells. J. Biol. Chem. **274**:22102–22108.
33. **Boyd AP, Lambermont I, Cornelis GR.** 2000. Competition between the Yops of *Yersinia enterocolitica* for delivery into eukaryotic cells: role of the SycE chaperone binding domain of YopE. J. Bacteriol. **182**:4811–4821.
34. **Elliott SJ, Wainwright LA, McDaniel TK, Jarvis KG, Deng YK, Lai LC, McNamara BP, Donnenberg MS, Kaper JB.** 1998. The complete sequence of the locus of enterocyte effacement (LEE) from enteropathogenic *Escherichia coli* E2348/69. Mol. Microbiol. **28**:1–4.
35. **Charpentier X, Oswald E.** 2004. Identification of the secretion and translocation domain of the enteropathogenic and enterohemorrhagic *Escherichia coli* effector Cif, using TEM-1 beta-lactamase as a new fluorescence-based reporter. J. Bacteriol. **186**:5486–5495.
36. **Iguchi A, Thomson NR, Ogura Y, Saunders D, Ooka T, Henderson IR, Harris D, Asadulghani M, Kurokawa K, Dean P, Kenny B, Quail MA, Thurston S, Dougan G, Hayashi T, Parkhill J, Frankel G.** 2009. Complete genome sequence and comparative genome analysis of enteropathogenic *Escherichia coli* O127:H6 strain E2348/69. J. Bacteriol. **191**:347–354.
37. **Mills E, Baruch K, Charpentier X, Kobi S, Rosenshine I.** 2008. Real-time analysis of effector translocation by the type III secretion system of enteropathogenic *Escherichia coli*. Cell Host Microbe **3**:104–113.
38. **Elliott SJ, O'Connell CB, Koutsouris A, Brinkley C, Donnenberg MS, Hecht G, Kaper JB.** 2002. A gene from the locus of enterocyte effacement that is required for enteropathogenic *Escherichia coli* to increase tight-junction permeability encodes a chaperone for EspF. Infect. Immun. **70**:2271–2277.
39. **Thomas NA, Deng W, Baker N, Puente J, Finlay BB.** 2007. Hierarchical delivery of an essential host colonization factor in enteropathogenic *Escherichia coli*. J. Biol. Chem. **282**:29634–29645.
40. **Delahay RM, Shaw RK, Elliott SJ, Kaper JB, Knutton S, Frankel G.** 2002. Functional analysis of the enteropathogenic *Escherichia coli* type III secretion system chaperone CesT identifies domains that mediate substrate interactions. Mol. Microbiol. **43**:61–73.
41. **Keen NT, Tamaki S, Kobayashi D, Trollinger D.** 1988. Improved broad-host-range plasmids for DNA cloning in gram-negative bacteria. Gene **70**:191–197.
42. **Thomassin JL, He X, Thomas NA.** 2011. Role of EscU auto-cleavage in promoting type III effector translocation into host cells by enteropathogenic *Escherichia coli*. BMC Microbiol. **11**:205.
43. **Cirino PC, Mayer KM, Umeno D.** 2003. Generating mutant libraries using error-prone PCR. Methods Mol. Biol. **231**:3–9.
44. **Bradford MM.** 1976. A rapid and sensitive method for the quantitation of microgram quantities of protein utilizing the principle of protein-dye binding. Anal. Biochem. **72**:248–254.
45. **Rumpel S, Lakshmi R, Becker S, Zweckstetter M.** 2008. Assignment-free solution NMR method reveals CesT as an unswapped homodimer. Protein Sci. **17**:2015–2019.

46. **Papadopoulos JS, Agarwala R.** 2007. COBALT: constraint-based alignment tool for multiple protein sequences. Bioinformatics **23**:1073–1079.
47. **Vingadassalom D, Campellone KG, Brady MJ, Skehan B, Battle SE, Robbins D, Kapoor A, Hecht G, Snapper SB, Leong JM.** 2010. Enterohemorrhagic *E. coli* requires N-WASP for efficient type III translocation but not for EspFU-mediated actin pedestal formation. PLoS Pathog. **6**:e1001056. doi:10.1371/journal.ppat.1001056.
48. **Gruenheid S, Sekirov I, Thomas NA, Deng W, O'Donnell P, Goode D, Li Y, Frey EA, Brown NF, Metalnikov P, Pawson T, Ashman K, Finlay BB.** 2004. Identification and characterization of NleA, a non-LEE-encoded type III translocated virulence factor of enterohaemorrhagic *Escherichia coli* O157:H7. Mol. Microbiol. **51**:1233–1249.
49. **Deng W, Li Y, Hardwidge PR, Frey EA, Pfuetzner RA, Lee S, Gruenheid S, Strynakda NC, Puente JL, Finlay BB.** 2005. Regulation of type III secretion hierarchy of translocators and effectors in attaching and effacing bacterial pathogens. Infect. Immun. **73**:2135–2146.
50. **Laemmli UK.** 1970. Cleavage of structural proteins during the assembly of the head of bacteriophage T4. Nature **227**:680–685.
51. **Yip CK, Kimbrough TG, Felise HB, Vuckovic M, Thomas NA, Pfuetzner RA, Frey EA, Finlay BB, Miller SI, Strynadka NC.** 2005. Structural characterization of the molecular platform for type III secretion system assembly. Nature **435**:702–707.
52. **Panina EM, Mattoo S, Griffith N, Kozak NA, Yuk MH, Miller JF.** 2005. A genome-wide screen identifies a *Bordetella* type III secretion effector and candidate effectors in other species. Mol. Microbiol. **58**:267–279.
53. **Samudrala R, Heffron F, McDermott JE.** 2009. Accurate prediction of secreted substrates and identification of a conserved putative secretion signal for type III secretion systems. PLoS Pathog. **5**:e1000375. doi:10.1371/journal.ppat.1000375.
54. **Arnold R, Brandmaier S, Kleine F, Tischler P, Heinz E, Behrens S, Niinikoski A, Mewes HW, Horn M, Rattei T.** 2009. Sequence-based prediction of type III secreted proteins. PLoS Pathog. **5**:e1000376. doi:10.1371/journal.ppat.1000376.
55. Reference deleted.
56. **Niesen FH, Berglund H, Vedadi M.** 2007. The use of differential scanning fluorimetry to detect ligand interactions that promote protein stability. Nat. Protoc. **2**:2212–2221.
57. **Knubovets T, Osterhout JJ, Connolly PJ, Klibanov AM.** 1999. Structure, thermostability, and conformational flexibility of hen egg-white lysozyme dissolved in glycerol. Proc. Natl. Acad. Sci. U. S. A. **96**:1262–1267.
58. **Thanabalasuriar A, Koutsouris A, Weflen A, Mimee M, Hecht G, Gruenheid S.** 2010. The bacterial virulence factor NleA is required for the disruption of intestinal tight junctions by enteropathogenic *Escherichia coli*. Cell. Microbiol. **12**:31–41.
59. **Birtalan SC, Phillips RM, Ghosh P.** 2002. Three-dimensional secretion signals in chaperone-effector complexes of bacterial pathogens. Mol. Cell **9**:971–980.
60. **Stebbins CE, Galan JE.** 2001. Maintenance of an unfolded polypeptide by a cognate chaperone in bacterial type III secretion. Nature **414**:77–81.
61. **Koide S, Sidhu SS.** 2009. The importance of being tyrosine: lessons in molecular recognition from minimalist synthetic binding proteins. ACS Chem. Biol. **4**:325–334.
62. **Fraser GM, Bennett JC, Hughes C.** 1999. Substrate-specific binding of hook-associated proteins by FlgN and FliT, putative chaperones for flagellum assembly. Mol. Microbiol. **32**:569–580.
63. **Minamino T, Kinoshita M, Hara N, Takeuchi S, Hida A, Koya S, Glenwright H, Imada K, Aldridge PD, Namba K.** 2012. Interaction of a bacterial flagellar chaperone FlgN with FlhA is required for efficient export of its cognate substrates. Mol. Microbiol. **83**:775–788.
64. **Garcia-Angulo VA, Deng W, Thomas NA, Finlay BB, Puente JL.** 2008. Regulation of expression and secretion of NleH, a new non-locus of enterocyte effacement-encoded effector in *Citrobacter rodentium*. J. Bacteriol. **190**:2388–2399.
65. **Li M, Rosenshine I, Yu HB, Nadler C, Mills E, Hew CL, Leung KY.** 2006. Identification and characterization of NleI, a new non-LEE-encoded effector of enteropathogenic *Escherichia coli* (EPEC). Microbes Infect. **8**:2890–2898.
66. **Sorg JA, Blaylock B, Schneewind O.** 2006. Secretion signal recognition by YscN, the *Yersinia* type III secretion ATPase. Proc. Natl. Acad. Sci. U. S. A. **103**:16490–16495.
67. **Auvray F, Ozin AJ, Claret L, Hughes C.** 2002. Intrinsic membrane targeting of the flagellar export ATPase FliI: interaction with acidic phospholipids and FliH. J. Mol. Biol. **318**:941–950.
68. **Lorenz C, Buttner D.** 2009. Functional characterization of the type III secretion ATPase HrcN from the plant pathogen *Xanthomonas campestris* pv. *vesicatoria*. J. Bacteriol. **191**:1414–1428.
69. **Riordan KE, Sorg JA, Berube BJ, Schneewind O.** 2008. Impassable YscP substrates and their impact on the *Yersinia enterocolitica* type III secretion pathway. J. Bacteriol. **190**:6204–6216.
70. **Biemans-Oldehinkel E, Sal-Man N, Deng W, Foster LJ, Finlay BB.** 2011. Quantitative proteomic analysis reveals formation of an EscL-EscQ-EscN type III complex in enteropathogenic *Escherichia coli*. J. Bacteriol. **193**:5514–5519.